

**A peer-reviewed version of this preprint was published in PeerJ on 26 July 2016.**

[View the peer-reviewed version](https://peerj.com/articles/2242) (peerj.com/articles/2242), which is the preferred citable publication unless you specifically need to cite this preprint.

Ledogar JA, Dechow PC, Wang Q, Gharpure PH, Gordon AD, Baab KL, Smith AL, Weber GW, Grosse IR, Ross CF, Richmond BG, Wright BW, Byron C, Wroe S, Strait DS. 2016. Human feeding biomechanics: performance, variation, and functional constraints. PeerJ 4:e2242 <https://doi.org/10.7717/peerj.2242>

# 1 Human feeding biomechanics: performance, variation, and 2 functional constraints

3  
4

5 Justin A. Ledogar<sup>1,2</sup>, Paul C. Dechow<sup>3</sup>, Qian Wang<sup>3</sup>, Poorva Gharpure<sup>3</sup>, Adam D. Gordon<sup>2</sup>,  
6 Karen L. Baab<sup>4</sup>, Amanda L. Smith<sup>2,5</sup>, Gerhard W. Weber<sup>6</sup>, Ian R. Grosse<sup>7</sup>, Callum F. Ross<sup>8</sup>,  
7 Brian G. Richmond<sup>9,10</sup>, Barth W. Wright<sup>11</sup>, Craig Byron<sup>12</sup>, Stephen Wroe<sup>2</sup>, David S. Strait<sup>2,5</sup>

8  
9

10 <sup>1</sup>Zoology Division, School of Environmental and Rural Science, University of New England,  
11 Armidale, NSW, Australia

12 <sup>2</sup>Department of Anthropology, University at Albany, Albany, NY, USA

13 <sup>3</sup>Department of Biomedical Sciences, Texas A&M University, Baylor College of Dentistry,  
14 Dallas, TX, USA

15 <sup>4</sup>Department of Anatomy, Midwestern University, Glendale, AZ, USA

16 <sup>5</sup>Department of Anthropology, Washington University in St. Louis, St. Louis, MO, USA

17 <sup>6</sup>Department of Anthropology, University of Vienna, Vienna, Austria

18 <sup>7</sup>Department of Mechanical & Industrial Engineering, University of Massachusetts, Amherst,  
19 MA, USA

20 <sup>8</sup>Department of Organismal Biology & Anatomy, University of Chicago, Chicago, IL, USA

21 <sup>9</sup>Division of Anthropology, American Museum of Natural History, New York, NY, USA

22 <sup>10</sup>Department of Human Evolution, Max Planck Institute for Evolutionary Anthropology,  
23 Leipzig, Germany

24 <sup>11</sup>Department of Anatomy, Kansas City University of Medicine and Biosciences, Kansas City,  
25 MO, USA

26 <sup>12</sup>Department of Biology, Mercer University, Macon, GA, USA

27  
28

Corresponding Author:

29  
30

Justin A. Ledogar<sup>1,2</sup>

31  
32

Zoology Division, School of Environmental and Rural Science

33 University of New England

34 Armidale, NSW 2351

35 Australia

36  
37

Email: [jledogar@une.edu.au](mailto:jledogar@une.edu.au)

38 Phone: +61 2 6773 5896

39  
40

41  
42

43  
44

45

46 **ABSTRACT**

47           The evolution of the modern human (*Homo sapiens*) cranium is characterized by a  
48 reduction in the size of the feeding system, including reductions in the size of the facial skeleton,  
49 postcanine teeth, and the muscles involved in biting and chewing. The conventional view  
50 hypothesizes that gracilization of the human feeding system is related to a shift toward eating  
51 foods that were less mechanically challenging to consume and/or foods that were processed  
52 using tools before being ingested. This hypothesis predicts that human feeding systems should  
53 not be well-configured to produce forceful bites and that the cranium should be structurally  
54 weak. An alternate hypothesis states that the modern human face is adapted to generate and  
55 withstand high biting forces. We used finite element analysis (FEA) to test two opposing  
56 mechanical hypotheses: that compared to our closest living relative, chimpanzees (*Pan*  
57 *troglydytes*), the modern human craniofacial skeleton is 1) less well configured, or 2) better  
58 configured to generate and withstand high magnitude bite forces. We considered intraspecific  
59 variation in our examination of human feeding biomechanics by examining a sample of  
60 geographically diverse crania that differed notably in shape. We found that our biomechanical  
61 models of human crania had broadly similar mechanical behavior despite their shape variation  
62 and were, on average, less structurally stiff than the crania of chimpanzees during unilateral  
63 biting when loaded with physiologically-scaled muscle loads. Our results also show that modern  
64 humans are efficient producers of bite force, consistent with previous analyses. However, highly  
65 tensile reaction forces were generated at the working (biting) side jaw joint during unilateral  
66 molar bites in which the chewing muscles were recruited with bilateral symmetry. In life, such a  
67 configuration would have increased the risk of joint dislocation and constrained the maximum  
68 recruitment levels of the masticatory muscles on the balancing (non-biting) side of the head. Our

69 results do not necessarily conflict with the hypothesis that anterior tooth (incisors, canines,  
70 premolars) biting could have been selectively important in humans, although the reduced size of  
71 the premolars in humans has been shown to increase the risk of tooth crown fracture. We  
72 interpret our results to suggest that human craniofacial evolution was probably not driven by  
73 selection for high magnitude unilateral biting, and that increased masticatory muscle efficiency  
74 in humans is likely to be a secondary byproduct of selection for some function unrelated to  
75 forceful biting behaviors. These results are consistent with the hypothesis that a shift to softer  
76 foods and/or the innovation of pre-oral food processing techniques relaxed selective pressures  
77 maintaining craniofacial features favoring forceful biting and chewing behaviors, leading to the  
78 characteristically small and gracile faces of modern humans.

79

80

81

82

83

84

85

86

87

88

89

90

91

92

93

94 **INTRODUCTION**

95 Human craniofacial architecture is extreme among living primate species. In particular,  
96 modern humans (*Homo sapiens*) exhibit a tall braincase and a small and short maxilla which  
97 distinguishes them from even our closest living relatives, the chimpanzees and bonobos of genus  
98 *Pan* (Fleagle, Gilbert & Baden, 2010). Reductions in the size and prognathism of the face,  
99 combined with increases in neurocranial globularity, have also been shown to differentiate  
100 modern humans from some extinct members of the genus *Homo* (Lieberman, McBratney &  
101 Krovitz, 2002). *Homo* exhibits an even more pronounced reduction in the size and robusticity of  
102 the facial skeleton, as well as in the size of the postcanine dentition and masticatory muscles  
103 (e.g., Robinson, 1954; Rak, 1983; Demes & Creel, 1988), relative to australopiths, an extinct  
104 informal group of early hominins from which modern humans are likely to be descended (e.g.,  
105 Walker, 1991; Wood, 1992; Skelton & McHenry, 1992; Strait, Grine & Moniz, 1997; Strait &  
106 Grine, 2004; Kimbel, Rak & Johanson, 2004; Berger et al., 2010). Theories purporting to explain  
107 the adaptive significance of masticatory reduction in *Homo* frequently stress the importance of  
108 changes in diet, usually involving a shift to foods that require less extensive intra-oral processing  
109 (e.g., Robinson, 1954; Rak, 1983; Brace, Smith & Hunt, 1991; Wrangham et al., 1999;  
110 Lieberman et al., 2004; Ungar, Grine & Teaford, 2006; Wood, 2009). However, Wroe et al.  
111 (2010) suggest that modern human crania are instead adapted to produce forceful bites, based on  
112 their conclusion that the human feeding apparatus is mechanically efficient, requires less muscle  
113 force than most other hominoids in order to generate comparable bite reaction forces, and should

114 therefore require a less robust structure. This paper evaluates these two alternatives by  
115 comparing feeding biomechanics in modern *H. sapiens* to that of chimpanzees (*Pan troglodytes*).

116 A conventional view of cranial gracilization in the lineage leading to modern *Homo* states  
117 that this process was spurred by the development of stone tool technologies (e.g., Ungar, Grine  
118 & Teaford, 2006), as tool use reduces food particle size (Lucas, 2004), allowing a reduced bite  
119 force per chew and/or fewer chews per feeding bout (Lucas & Luke, 1984; Agrawal et al., 1997;  
120 Zink & Lieberman, 2016). Under this hypothesis, tool use reduces the selective advantage  
121 offered by anatomical features that increase muscle force leverage and/or buttress the face  
122 against feeding loads. In addition to tool use, increased reliance on meat eating may have played  
123 a role in the initial stages of masticatory reduction in early *Homo* (Lieberman, 2008; Ungar,  
124 2012; Zink & Lieberman, 2016). Further gracilization of the jaws and teeth is hypothesized to  
125 have occurred with the advent of cooking, which may have been practiced by *H. erectus*  
126 (Wrangham, 2009; Organ et al., 2011), by reducing masticatory stresses (Lieberman et al., 2004;  
127 Lucas, 2004) and increasing digestive efficiency (Wrangham et al., 1999; Carmody &  
128 Wrangham, 2009; Carmody, Weintraub & Wrangham, 2011; Groopman, Carmody &  
129 Wrangham, 2015). If gracilization in *Homo* is a consequence of the removal of selection pressure  
130 to maintain and resist high magnitude or repetitive bite forces, then human feeding systems  
131 should not be optimized to produce high biting forces and the cranium could be structurally weak  
132 (i.e., exhibit high stress and strain when exposed to feeding loads).

133 The hypothesis described above is opposed by an alternative interpretation of human  
134 feeding mechanics. A paradox of the human cranium is that the marked facial orthognathism  
135 exhibited by recent modern humans increases the mechanical advantage (i.e., leverage) of the  
136 muscles responsible for elevating the mandible, allowing humans to generate a given bite force

137 with relatively low muscular effort (Spencer & Demes, 1993; O'Connor, Franciscus & Holton,  
138 2005; Lieberman, 2008, 2011; Wroe et al., 2010; Eng et al., 2013). Many studies interpret bite  
139 force efficiency among primate species as being significant in an adaptive sense (Rak, 1983;  
140 Strait et al., 2013; Smith et al., 2015a; Ross & Iriarte-Diaz, 2014), with increases in leverage  
141 predicted for species that rely on foods that require forceful biting in order to be processed (e.g.,  
142 hard seeds or nuts). Therefore, high biting leverage among humans seemingly contrasts with the  
143 hypothesis that the human craniofacial skeleton has experienced relaxed selection for traits that  
144 favor forceful biting and chewing behaviors (e.g., Brace, Smith & Hunt, 1991; Lieberman et al.,  
145 2004; Ungar, Grine & Teaford, 2006; Wood, 2009). However, Wroe et al. (2010) present an  
146 alternative view based on their analysis of modern human, extant ape, and fossil australopith  
147 feeding biomechanics. Using finite element analysis (FEA), Wroe et al. (2010) found that their  
148 human model was mechanically more efficient at producing bite forces than the other hominoids  
149 in their sample. Additionally, they found that the human cranium experienced stresses similar to  
150 those in 3 of the 5 other species when models were scaled to the same surface area and bite force,  
151 including *Pan*. Consequently, Wroe et al. (2010) conclude that the human skull need not be as  
152 robust in order to generate, or sustain, bite reaction forces comparable to those of other  
153 hominoids, and that powerful biting behaviors may have been selectively important in shaping  
154 the modern human cranium.

155         Here, we use FEA to test two opposing mechanical hypotheses: that relative to  
156 chimpanzees, the modern human craniofacial skeleton is 1) less well configured, or 2) better  
157 configured to *generate* and *withstand* high magnitude unilateral bite forces. Our analysis builds  
158 on previous research into human craniofacial function (e.g., Lieberman, 2008; Wroe et al., 2010;  
159 Szwedowski, Fialkov & Whyne, 2011; Maloul et al., 2012) by examining masticatory

160 biomechanics within the context of the constrained lever model (Greaves, 1978; Spencer and  
161 Demes, 1993; Spencer, 1998, 1999), which predicts that bite force production in mammals is  
162 constrained by the risk of generating distractive (tensile) forces at the working (biting) side TMJ.  
163 Under this model, during unilateral biting, reaction forces are produced at the bite point and the  
164 working and balancing (non-biting) side TMJs. These three points form a “triangle of support”,  
165 and the line of action of the resultant vector of the jaw elevator muscle forces must intersect this  
166 triangle in order to produce a “stable” bite in which compressive reaction forces are generated at  
167 all three points (Fig. 1A). The resultant vector lies in the midsagittal plane when the muscles are  
168 recruited with bilateral symmetry and will pass through the triangle of support during bites on  
169 the incisors, canines, and premolars. However, molar biting changes the shape of the triangle  
170 such that a midline muscle result may lie outside of the triangle of support. If this occurs, a  
171 distractive (tensile) force is generated in the working side TMJ that “pulls” the mandibular  
172 condyle from the articular eminence (Fig. 1B). In the case of the mammalian jaw, the soft tissues  
173 of the TMJ are well suited to resist compressive joint reaction forces in which the mandibular  
174 condyle is being “driven” into the cranium, but they are poorly configured to resist distractive  
175 joint forces in which the condyle is being “pulled away” from the cranium (Greaves, 1978).  
176 Mammals, including humans (Spencer, 1998), avoid this by reducing the activity of the chewing  
177 muscles on the balancing side during bites on the posterior teeth. This draws the muscle resultant  
178 vector toward the working side and back within the triangle, but the total muscle force available  
179 for biting is reduced, thereby reducing peak bite force magnitudes. Thus, although one might  
180 expect that a bite on a distal tooth would produce an elevated bite force due to a short load arm  
181 (per a given muscle force), this effect is mitigated by the constraint that the muscle force vector  
182 must lie within the triangle of support. A finding that constraints on bite force production were



183 especially strong in humans would be consistent with the hypothesis that the human cranium is  
184 poorly configured to generate high unilateral bite forces, and inconsistent with the opposing  
185 hypothesis.

186 We further build on previous work by considering intraspecific variation in our analysis  
187 of human feeding biomechanics. Our prior work has shown that high degrees of intraspecific  
188 variation in cranial shape need not necessarily produce a high degree of intraspecific mechanical  
189 variation (Smith et al., 2015b), implying that mechanical patterns are conservative and reflect an  
190 underlying common geometry that may be overlain by skeletal traits that can vary without  
191 dramatically altering the fundamental mechanical framework of the cranium. A caveat, however,  
192 is that Smith et al. (2015b) examined only one species, *P. troglodytes*. Thus, it has yet to be  
193 established if this pattern is generalizable across primates (or other vertebrates). Accordingly, we  
194 examined mechanical variation among a sample of geographically diverse human crania found to  
195 differ notably in shape.

196

## 197 MATERIALS & METHODS

### 198 Analysis of human cranial shape variation and selection of specimens for FEA

199 We analyzed finite element models (FEMs) of six crania lying at the extremes of human  
200 variation, as well as one “average” specimen found to conform closely to an average shape. To  
201 select specimens, we analyzed shape variation within a sample of modern human (*H. sapiens*)  
202 crania using previously collected geometric morphometric (GM) data (Baab et al., 2010). We  
203 analyzed 85 landmarks collected from a sample of 88 Holocene human crania housed at the  
204 American Museum of Natural History (AMNH) (Tables 1, 2). These included mainly facial  
205 landmarks combined with a few that characterize neurocranial shape, corresponding to our focus

206 on facial biomechanics in this study. This sample includes individuals from diverse regions  
207 across the globe, and provides a cross-section of populations that differ in cranial robusticity  
208 (Baab et al., 2010). Landmark data from these 88 specimens were converted to shape coordinates  
209 by Generalized Procrustes analysis (e.g., Bookstein, 1991; Slice, 2005) and analyzed using  
210 principal components analysis (PCA). We found that the first 3 principal components (PCs)  
211 described 39% of the shape variation in our sample (Fig. 2). In order to maximize shape-related  
212 biomechanical variation in our FEMs, we considered variation from all 88 PCs when selecting  
213 specimens to be modeled. We first determined those individuals exhibiting the largest distances  
214 from the group centroid (i.e., consensus shape), calculated as Euclidean distance using all 88 PCs  
215 (Table 3). From among these individuals, we chose the six specimens that exhibited the largest  
216 pairwise distances, excluding insufficiently preserved crania, those missing many teeth, and  
217 those unavailable for loan (Table 4). These six “extreme” modern human crania included: one  
218 male and one female Khoe-San from South Africa (AMNH VL/2463 and AMNH VL/2470,  
219 hereafter referred to as “KSAN1” and “KSAN2”); a male from Greifenberg, Austria (AMNH  
220 VL/3878, “BERG”); a female from the Malay Archipelago (AMNH 99/7889, “MALP”); a male  
221 from the Tigara culture at Point Hope, Alaska (AMNH 99.1/511, “TIGA”); and a male from  
222 Ashanti, West Africa (AMNH VL/1602, “WAFR”). An additional specimen, a Native American  
223 male from Grand Gulch, Utah (AMNH 99/7365, “GRGL”), was chosen as an “average”  
224 representative of human cranial shape based on its close proximity (i.e., small Euclidean  
225 distance) to the group centroid and its availability for loan (see Table 3). Note that this individual  
226 was incorrectly transcribed as AMNH 99/7333 by Ledogar (2015).

227

228 **Creation of finite element models from “extreme” and “average” human specimens**

229 *Construction of solid models*

230           The seven specimens chosen for analysis were CT-scanned at Penn State’s Center for  
231 Quantitative Imaging (pixel size = 0.16 mm) and the 2D digital image stacks were used to create  
232 seven solid meshes (Fig. 3) using Mimics v 14.0 (Materialise, Ann Arbor, MI, USA), following  
233 the methods outlined by Smith et al., 2015 (a,b). Mandibles corresponding to the seven crania  
234 (except for BERG and KSAN2, which lacked mandibles; see below) were also scanned so that  
235 they could be used to direct muscle force vectors in the loading simulations described below. The  
236 crania were solid-meshed at similar densities using tet4 elements (element count:  
237 GRGL=2,118,350; BERG=1,928,931; KSAN1=1,620,112; KSAN2=1,392,417;  
238 MALP=1,323,093; TIGA=2,059,433; WAFR=1,831,053). Solid meshes were then imported as  
239 Nastran (NAS) files into Strand7 (Strand7 Pty Ltd) FEA software.

240           We created two sets of human FEMs that differed in their assigned muscle force and  
241 bone properties. One set of human FEMs (“ALL-HUM” models) was assigned human properties  
242 for bone tissue and masticatory muscle force, whereas chimpanzee properties were applied to the  
243 second set (“CHIMPED” models). The ALL-HUM models provide the most realistic assessment  
244 of human cranial mechanics, in terms of the predicted strains and bite forces. These models also  
245 allow for a more thorough examination of intraspecific variation in humans. In contrast, the  
246 CHIMPED models permit direct comparisons between our humans FEMs and our previously  
247 analyzed FEMs of chimpanzees and fossil hominins (Smith et al., 2015a,b). These comparisons  
248 focus on shape-related differences in mechanical performance that are free of the effects of  
249 differences in cranial size and bone material properties. Therefore, the comparisons between the  
250 CHIMPED human models and the chimpanzee data from Smith et al. (2015a,b) most directly

251 address our mechanical hypothesis described above because the hypotheses relate specifically to  
252 the mechanical consequences of shape differences.

253

#### 254 *Material properties of tissues*

255 Human cortical bone material properties assigned to the ALL-HUM models were  
256 collected from various locations across the craniofacial skeletons of two fresh-frozen human  
257 cadavers (female, aged 22; male, aged 42) by measuring their resistance to ultrasonic wave  
258 propagation (see Supplementary Information). Previous studies show that freezing has only a  
259 very minimal effect on ultrasonic measurements and elasticity of cortical bone (Zioupos et al.,  
260 2000). For each location sampled, the elastic (Young's) modulus in the axis of maximum  
261 stiffness ( $E3$ ) was averaged between the human donors and used to distribute spatially  
262 heterogeneous isotropic material properties throughout the seven human FEMs using a method  
263 (Davis et al., 2011) analogous to the diffusion of heat through a highly conductive material. To  
264 achieve this, values at each of the sampled locations, which ranged from 17.92 GPa to 25.52 GPa  
265 (mean=20.61 GPa, SD=1.92), were converted to temperatures and distributed throughout the  
266 cortical volume of the FEM. The elastic modulus of cortical bone was then set to vary with  
267 temperature during the subsequent loading analysis, with any thermally-induced strains removed  
268 from the analysis. For Poisson's ratios, models were each assigned the average of the sampled  
269 locations ( $\nu_{23} = 0.293$ ). The same procedure was used to diffuse chimpanzee material properties  
270 to the CHIMPED model variants using data collected from a cadaveric female chimpanzee at 14  
271 craniofacial regions (Smith et al., 2015a,b). In both the ALL-HUM and CHIMPED sets of model  
272 variants, homogeneous isotropic properties were used to model both trabecular bone ( $E3=637$   
273 MPa;  $\nu_{23}=0.28$ ) and enamel ( $E3=80,000$  MPa;  $\nu_{23}=0.28$ ), following Smith et al. (2015a,b).

274

275 *Muscle forces and constraints*

276           Jaw adductor muscle forces were applied to both sets of FEMs for the anterior  
277 temporalis, superficial masseter, deep masseter, and medial pterygoid under the assumption that  
278 the chewing muscles were acting at peak activity levels on both sides of the cranium. These  
279 loads allow an estimate of the maximum bite force produced by each individual. In the ALL-  
280 HUM variants, muscle forces were applied based on muscle physiological cross-sectional area  
281 (PCSA) data reported by van Eijden, Korfagen & Brugman (1997), with forces corrected to  
282 account for pennation and differences in gape during fixation using formulae from Taylor &  
283 Vinyard (2013). Corrected PCSAs were then used to calculate forces in Newtons (N) such that  
284 each  $\text{cm}^2$  of muscle was equivalent to 30 N (Murphy, 1998). These unscaled forces were applied  
285 to the “average” specimen (GRGL), while the six “extreme” variants were applied forces that  
286 were either scaled up or down based on differences in model size (Table 5), with size represented  
287 by model volume (i.e., the summed volume of all tet4 elements in  $\text{mm}^3$ ) to the two-thirds power.  
288 This muscle force scaling procedure removes the effects of differences in model size on stress,  
289 strain, and strain energy density from the mechanical results (Dumont, Grosse & Slater, 2009;  
290 Strait et al., 2010). The CHIMPED model variants were also assigned forces that were scaled  
291 dependent on their size using PCSA data from an adult female chimpanzee (Strait et al., 2009;  
292 Smith et al., 2015a,b). However, rather than scaling the FEMs around the “average” specimen  
293 (GRGL), we scaled the forces applied to the CHIMPED models (see Table 5) from the baseline  
294 chimpanzee model used for scaling purposes (PC1+) in the analysis by Smith et al. (2015b),  
295 permitting size-free comparisons between humans and chimps. For both sets of muscle loadings,  
296 plate elements modeled as 3D membrane were “zipped” at their nodes to the surface faces of tet4

297 elements representing each muscle's origin. The scaled muscle forces for each set of analyses  
298 were applied using Boneload (Grosse et al., 2007) to the normal surfaces of the plate elements as  
299 tractions directed toward their respective insertions on the mandible, with the mandible slightly  
300 depressed and the condyles translated onto the articular eminences (Dumont, Piccirillo & Grosse,  
301 2010). Mandibles were only used here to direct these vectors. In the case of the BERG specimen,  
302 which was lacking its mandible, a scaled version of the GRGL mandible was used to define the  
303 orientation of muscle force vectors. Similarly, a scaled version of the KSAN1 mandible was used  
304 to replace the missing mandible in KSAN2.

305         For both sets of biting simulations, each of the seven FEMs was oriented such that one of  
306 three axes (i.e., X, Y, or Z) was parallel to the occlusal plane. Each model was constrained at a  
307 single node against translation in all axes at the working-side TMJ, while the balancing-side TMJ  
308 was constrained only in the superoinferior and anteroposterior directions (Strait et al., 2009;  
309 Smith et al., 2015a,b), thus creating an axis of rotation around the TMJs. Models were subjected  
310 to simulations of left premolar (P<sup>3</sup>) and left molar (M<sup>2</sup>) biting by constraining a node in the  
311 center of occlusal surface in each tooth, respectively, in the superoinferior direction. These  
312 constraints generated strains in the craniofacial skeleton, as well as reaction forces at the TMJs  
313 and bite point, upon the application of muscle forces.

314

#### 315 *Analysis of model output parameters*

316         Following Smith et al (2015a,b), we displayed global strain patterns using strain maps.  
317 These maps are analogous to histograms in that they illustrate strain magnitudes at thousands of  
318 nodes simultaneously, but have the added advantage of preserving spatial information. In  
319 addition, we collected strain data generated by each FEM from surface elements at 14 locations

320 across the craniofacial skeleton (Fig. 4). These locations correspond to those included in  
321 previous *in vitro* and *in silico* (e.g., FEA) studies on primate feeding biomechanics (e.g.,  
322 Hylander and Johnson, 1991, 1997; Ross et al., 2011; Smith et al., 2015a,b). At each location, we  
323 examined several strain metrics from each of the seven FEMs in order to understand patterns of  
324 deformation. These included maximum principal strain (tension), minimum principal strain  
325 (compression), maximum shear strain (maximum principal strain – minimum principal strain),  
326 von Mises strain (distortional strain or non-isometric strain), and strain energy density (SED, the  
327 strain energy stored at a given point). Additionally, strain mode, the absolute value of maximum  
328 principal strain divided by minimum principal strain, was recorded for each location. This  
329 measure indicates whether tension or compression is dominant at a given location.

330 Data on the reaction forces generated at constrained nodes (i.e., the bite point and two  
331 TMJs) were recorded in Newtons (N). Reaction forces at the P<sup>3</sup> and M<sup>2</sup> were recorded relative to  
332 the occlusal plane, while reaction forces at the left and right TMJs were recorded and compared  
333 relative to a user-defined “triangle of support” Cartesian coordinate system, with one of three  
334 axes perpendicular to a reference plane defined by the “triangle of support” formed by the  
335 constrained nodes at the bite point and two articular eminences (Smith et al., 2015a,b). The  
336 efficiency of bite force production at a given bite point in each model was also compared using  
337 the mechanical advantage (MA), a measure of masticatory muscle efficiency or leverage,  
338 calculated as the ratio of bite force output to muscle force input.

339 In the evaluation of our mechanical hypothesis, we first inspected data collected from the  
340 ALL-HUM models for large levels of intraspecific variation that could potentially invalidate the  
341 functional significance of our results. Strain magnitudes and SED at each of the 14 sampled  
342 locations were examined for large differences between individuals, in addition to a comparison

343 of coefficients of variation (CVs) at specific locations. Differences in the spatial patterning of  
344 strain magnitudes between the ALL-HUM models were also compared using strain maps, in  
345 addition to variation in biting efficiency (i.e., MA). Lastly, we also calculated CVs for von Mises  
346 strain and MA in the CHIMPED model variants for direct comparison with the chimpanzee CVs  
347 reported by Smith et al. (2015b) using the Fligner-Killeen test for equal CVs.

348 To analyze relative mechanical performance in our human FEMs, we focused on  
349 comparisons between the CHIMPED humans and our previously analyzed FEMs of chimpanzee  
350 crania (Smith et al., 2015b). Specifically, we compared the magnitudes of von Mises strain,  
351 considered to be a key metric in assessing regional bone strength (Keyak & Rossi, 2000), at the  
352 14 sampled locations, as well as differences in biting efficiency, between humans and chimps.  
353 We tested for significant differences between species using the Mann-Whitney  $U$  test.

354

### 355 ***In vitro* validation of specimen-specific human cranial FEM**

356 Data on *in vitro* bone strain collected during simulated P<sup>3</sup> biting in a cadaveric human  
357 head were used to validate our results. As noted above, two human heads were used to gather  
358 data on the properties of craniofacial cortical bone. Before the removal of bone samples, the  
359 male specimen was CT-scanned, and strain data from 14 craniofacial locations were collected  
360 during a series of *in vitro* loading analyses (see Supplementary Information). Digital images of  
361 the specimen were then used to construct an eighth FEM, the *in vitro* loadings were replicated  
362 using FEA, and strain data were collected from the FEM at locations corresponding to the 14  
363 gage sites. The *in vitro* and *in silico* strain data were then compared in order to establish the  
364 degree to which assumptions regarding geometry and material properties introduce error into an  
365 FEM, where error is represented by the differences between the *in vitro* (observed) and *in silico*



366 (expected) results, divided by the expected results. These data were also analyzed using ordinary  
367 least squares (OLS) regression. Lastly, the orientations for both maximum and minimum  
368 principal strain in FEM were visually compared to those recorded during the *in vitro* loadings.

369

## 370 RESULTS

### 371 *In vitro* validation of specimen-specific human cranial FEM

372 Strain magnitudes recorded during *in vitro* P<sup>3</sup> loadings of the human cadaveric specimen  
373 and the results of the specimen-specific FEA are listed in Table 6. Comparisons of these data  
374 reveal that the specimen-specific FEM generated strains very similar in magnitude to those  
375 generated during the *in vitro* loadings. Results of the regression analysis on log-transformed  
376 strain data confirm a close correspondence between *in vitro* and *in silico* results, with significant  
377 regressions of  $0.845x+0.194$  ( $r^2=0.909$ ,  $p<0.001$ ) and  $0.849x+0.186$  ( $r^2=0.953$ ,  $p<0.001$ ) for  
378 maximum principal strain and minimum principal strain, respectively. However, assumptions  
379 regarding geometry and material properties did introduce error into the FEM (see Table 6).  
380 Visual inspection of principal strain orientations in the specimen-specific FEA reveals that  
381 orientations for both maximum principal strain and minimum principal strain at the 14 sampled  
382 locations were also very similar to those recorded from the 14 gage locations during the *in vitro*  
383 analysis (Fig. S3 – Fig. S7).

384

### 385 Shape-related variation in human feeding biomechanics

#### 386 *Variation in strain magnitude and spatial patterning*

387 Box-plots of strain and SED distributions recorded from the ALL-HUM models at the 14  
388 sampled locations during premolar (P<sup>3</sup>) and molar (M<sup>2</sup>) biting are shown in Fig. 5 (see also

389 Tables S1 and S2). Despite notable differences in craniofacial morphology between the models,  
390 comparisons of strain magnitudes reveal strong similarities. For P<sup>3</sup> biting, the highest strain  
391 magnitudes were experienced at the working nasal margin (Location 12), although on average  
392 higher tensile strain magnitudes were generated at the working and balancing postorbital bars  
393 (Locations 4 and 5). During M<sup>2</sup> biting, the working zygomatic root (Location 8) was subjected to  
394 the highest strain magnitudes, except that tension was greatest at the balancing postorbital bar.  
395 During both bites, low strain magnitudes were generated along the supraorbital torus (Locations  
396 1-3), the balancing zygomatic root (Location 9), balancing infraorbital (Location 11), and the  
397 zygomatic bodies (Locations 13 and 14). All FEMs of human crania were found to exhibit this  
398 general pattern.

399         Some regions of the face did exhibit large differences among individuals. In particular,  
400 the FEMs were found to differ in von Mises strain magnitude by as much as 210% at the nasal  
401 margin, which also has the highest CVs for all forms of strain during both P<sup>3</sup> and M<sup>2</sup> biting  
402 (Table 7), with the exception of minimum principal strain at the working dorsal orbital (Location  
403 2) and balancing infraorbital (Location 11) during P<sup>3</sup> biting, SED at the working dorsal orbital  
404 (Location 2) during P<sup>3</sup> biting, and the balancing zygomatic body (Location 14) for both bites.

405         Strain mode was nearly always compressive or tensile at a given location across the seven  
406 ALL-HUM models (Fig. 6), with a few exceptions. During premolar biting, only 3 locations  
407 varied with respect to strain mode (Locations 1, 10, 11), with only one FEM differing from the  
408 other models in each case. These three locations also differed in strain mode during molar biting,  
409 with Locations 1 and 10 exhibiting slightly higher levels of variation, in addition to variation in  
410 strain mode at Location 4.

411 By comparison with CHIMPED FEMs, humans were found to exhibit lower levels of  
412 shape-related variation in von Mises strain magnitude and lower CVs than chimpanzees at the 14  
413 sampled locations (Table 8). However, results of the Fligner-Killeen tests reveal that only 3 of  
414 the 14 “gage sites” exhibit significant differences in CV values. Specifically, humans were found  
415 to exhibit a significantly lower CV at the zygomatic arches during both P<sup>3</sup> and M<sup>2</sup> biting at the  
416 working infraorbital during P<sup>3</sup> biting.

417

#### 418 *Variation in the spatial patterning of strain concentrations*

419 Despite some large differences in strain magnitude, the spatial patterning of strain  
420 distributions was similar across the ALL-HUM models. The color maps during P<sup>3</sup> biting (Fig. 7)  
421 reveal two predominant deformation regimes that are common across the seven FEMs: (1)  
422 superior displacement of the anterior maxilla in proximity to the loaded P<sup>3</sup>, which creates highly  
423 tensile and compressive (hence highly shearing) strains surrounding the root of the nasal margin,  
424 compression along the nasal margin, and compression at the working zygomatic root; and (2)  
425 frontal bending of the zygomae under the inferiorly directed pulling action of the masticatory  
426 muscles, which generates tension at the zygomatic body and near the zygomaticomaxillary  
427 junction, particularly at the working-side, and deforms the orbit such that it is tensed along an  
428 inferolaterally-oriented axis and compressed along a superolaterally-oriented axis.

429 The color maps of strain patterning during M<sup>2</sup> biting were also generally similar across  
430 the ALL-HUM models (Fig. 8). As expected, all models exhibited lower strain magnitudes in the  
431 lower maxillary region during molar biting compared to premolar biting, but higher  
432 concentrations of compressive strain at the working zygomatic root. Molar biting was also  
433 associated with the same type of frontal bending, zygomatic torsion, and orbital deformation that

434 was observed for premolar biting, with relatively large concentrations of strain at the postorbital  
435 bars, orbital margins, and medial infraorbital.

436 In their study of chimpanzee biomechanical variation, Smith et al. (2015b) compared  
437 color maps of principal strain magnitudes in their 6 models with the scales normalized to an  
438 average of 10 landmarks (Locations 1-5, 8-12). They suggest that, by illuminating similarities  
439 and differences between individuals in the concentrations of relatively high and low strain  
440 concentrations through this normalization step, such “relative strain” maps strain may be  
441 particularly informative in comparative analyses of craniofacial function. When viewed in this  
442 manner (Fig. 9), the CHIMPED human models more clearly reveal a shared pattern of facial  
443 deformation that differs from that of chimpanzees under identical loading conditions, which was  
444 predominantly characterized by torsion of the zygoma and resulting orbital deformation under  
445 the inferiorly-directed masseteric muscle force.

446

#### 447 *Variation in bite force production and efficiency*

448 The ALL-HUM models exhibit moderate differences in bite force production and  
449 efficiency (mechanical advantage, MA) at P<sup>3</sup> and M<sup>2</sup> bite points (Table 9). With respect to bite  
450 force production, humans generated premolar bite forces that ranged from 333 to 507 N when  
451 loaded with scaled masticatory muscle forces. The MA range for premolar biting was 0.34-0.43  
452 with all but one individual (WAFR) occupying a narrower range of 0.39-0.43. Molar bite forces  
453 ranged from 496 to 756 N. In terms of leverage, most FEMs exhibited molar MAs of 0.57-0.64,  
454 but with the WAFR model again being considerably less efficient (0.53).

455 When compared to the chimpanzee data in Smith et al. (2015a), the CHIMPED human  
456 models analyzed here were found to exhibit somewhat lower ranges of variation in biting MA.

457 However, results of the Fligner-Killeen tests reveal no significant differences in CV values  
458 between the species at either the P<sup>3</sup> (chimp=8.67, human=5.65; p=0.18) or M<sup>2</sup> (chimp=8.11,  
459 human=6.67; p=0.13) bite point.

460

#### 461 *Variation in reaction forces generated at the temporomandibular joints*

462 During premolar biting, all seven of the ALL-HUM models generated strongly  
463 compressive reaction forces at both TMJs (see Table 9), similar to the results for chimpanzees  
464 (Smith et al., 2015b). However, unlike in chimpanzees, M<sup>2</sup> biting generated distractive (tensile)  
465 reaction forces at the working-side TMJ that would have “pulled” the mandibular condyle away  
466 from the articular eminence in five of the seven models. In order to remove distractive forces,  
467 these models required reductions in the muscle force applied to the balancing-side, which ranged  
468 from 5% to 15% (see Table 9). Interestingly, when loaded with chimpanzee muscle forces, all  
469 seven of the CHIMPED human models exhibit distractive forces in the working TMJ during M<sup>2</sup>  
470 biting, with larger muscle force reductions required to eliminate the distraction (see below).

471

#### 472 **Biomechanical “performance” of human feeding**

##### 473 *Structural stiffness of the human craniofacial skeleton*

474 Direct comparisons of shape-related mechanical performance between our human FEMs  
475 and our previously analyzed chimpanzee FEMs (Smith et al., 2015a,b) were permitted by the  
476 CHIMPED models. These comparisons reveal that the human craniofacial skeleton is less stiff  
477 and experiences von Mises strains that are elevated relative to those experienced by chimpanzees  
478 when subjected to identical loading conditions (Fig. 10). Several of the sampled locations were  
479 found to experience significantly higher magnitudes in humans during both P<sup>3</sup> and M<sup>2</sup> biting

480 following the results of Holm-Bonferroni-corrected Mann-Whitney  $U$  tests (Table 10). These  
481 included the working nasal margin (Location 12), postorbital bars (Locations 4 and 5), working  
482 zygomatic root (Location 8), and the working dorsal orbital (Location 2). However, strains at the  
483 mid-zygomatic arches in humans were within the range observed for chimpanzees (which are  
484 extremely variable). Additionally, human zygomatic bodies were found to be structurally stiff,  
485 with significantly lower von Mises strain magnitudes than chimpanzees.

486

#### 487 *Human bite force production and mechanical efficiency*

488 Analysis of our CHIMPED human FEMs reveals that human crania are capable of  
489 generating bite forces with higher mechanical efficiency than chimpanzees (Fig. 11). Pairwise  
490 comparisons using the Mann-Whitey  $U$  test demonstrate that these differences are significant at  
491 both P<sup>3</sup> ( $U=1.5$ ,  $z=-2.73$ , exact  $p=0.003$ ) and M<sup>2</sup> ( $U=1$ ,  $z=-2.79$ , exact  $p=0.002$ ) bite points.  
492 However, unlike chimpanzees, all seven of the CHIMPED human models generated highly  
493 distractive (tensile) reaction forces at the working-side TMJ during molar biting. Therefore,  
494 molar biting in humans increases the risk of having the muscle resultant vector fall outside the  
495 triangle of support. To bring the joint back into compression, a reduction in balancing side  
496 muscle force of 15%-30% was required (Table 11).

497

## 498 **DISCUSSION**

### 499 *In vitro* validation

500 In order to validate the findings of our mechanical analysis, we compared *in vitro* bone  
501 strain in a cadaveric human head during simulated P<sup>3</sup> biting to the results of a specimen-specific  
502 FEA. We found the results of our specimen-specific FEA corresponded quite well with *in vitro*

503 data. In addition to the notable similarities in strain orientation at the 14 sampled locations,  
504 results of the regression analysis reveal that FEA can predict *in vitro* strain magnitudes with a  
505 high degree of accuracy ( $r^2$  values  $>0.9$ ). Similarly, Nagasao et al. (2005) were able to validate a  
506 dry bone human cranium with a high degree of accuracy ( $r^2=0.989$ ). However, these authors  
507 examined only 2 gage sites and they simulated biting by applying forces to teeth, thus omitting  
508 the impact of muscle loading. A greater number of sites were included in an analysis by  
509 Szwedowski, Fialkov & Whyne (2011), who found that their FEM results predicted *in vitro* data  
510 with an  $r^2$  of 0.73. Toro-Ibacache et al. (2015) also applied point loads to a cadaveric human  
511 head and validated strains at two locations in a specimen-specific FEM, finding broad  
512 similarities.

513         Although we found excellent correspondence between *in vitro* and *in silico* results, it is  
514 clear that FEA does incorporate error (see Table 6). This error was deceptively large at some  
515 “gage sites,” particularly in areas of low strain. For example, error for maximum principal strains  
516 at the balancing dorsal orbital (Location 3) was 80%, but this represents a difference between  
517 experimental and FEA results of only 2.67 microstrain ( $\mu\epsilon$ ). Generally speaking, this is not a  
518 meaningful difference in the context of vertebrate feeding biomechanics, where some regions of  
519 the cranium can experience strain in the thousands of microstrain. However, some moderately  
520 strained areas exhibited high error percentages. In particular, the working infraorbital validated  
521 well for minimum principal strain, but error for maximum principal strain was nearly 50%. This  
522 discrepancy may be related to the morphology of the bone that forms the thin anterior wall of the  
523 maxillary sinus, which is susceptible to large modeling errors (Maloul, Fialkov & Whyne, 2011),  
524 or could be a result of simplifications to the thin bones of the nasal cavity (see Toro-Ibacache et  
525 al., 2015).

526

527 **Mechanical variation**

528           We found that the ALL-HUM models exhibited generally low levels of shape-related  
529 mechanical variation in strain magnitude and bite force production. Additionally, though some  
530 regions (e.g., the nasal margin) were found to exhibit large differences in strain magnitude, our  
531 human FEMs shared a common pattern of the spatial distribution of relatively high and low  
532 strain concentrations. These findings are similar to those of Smith et al. (2015b), who found  
533 broad similarities in strain patterning among on a sample of chimpanzee FEMs that differed  
534 notably in shape. Similarly, Toro-Ibacache, Zapata Muñoz & O'Higgins (2015) found broad  
535 similarities between two notably distinct human cranial FEMs. Our finding that the ALL-HUM  
536 models exhibit low levels of mechanical variation supports the functional significance of the  
537 comparisons of shape-related mechanical performance made between our CHIMPED human  
538 FEMs and our previously analyzed chimpanzee FEMs (Smith et al., 2015a,b), which focused  
539 purely on mechanical differences resulting from geometrical/architectural variation in the  
540 craniofacial skeleton.

541

542 **Mechanical performance in humans and chimpanzee**543 *Craniofacial strength: Is the human face weak?*

544           Our results suggest that the modern human craniofacial skeleton is structurally less  
545 strong, in terms of resistance to masticatory stress, than that of chimpanzees when subjected to  
546 identical loading conditions (i.e., same properties and constraints, muscle forces scaled to model  
547 size). In the CHIMPED variants of our human FEMs, most of the locations analyzed experienced  
548 von Mises strain magnitudes that were elevated relative to chimpanzees, in particular the



549 working nasal margin, the postorbital bars, the working zygomatic root, and the working dorsal  
550 orbital region. Exceptions to this pattern include the zygomatic arches, where strains were  
551 bracketed by the range of values seen in chimp FEMs, and the prominence of the zygomatic  
552 body (i.e., the “cheek bone”), which is apparently strong in modern humans.

553         During unilateral P<sup>3</sup> biting, the nasal margin of modern humans experienced von Mises  
554 strains that were on average more than 350% greater than chimpanzees. Similarly, previous  
555 investigations identify the “root” of the nasal margin to be an area of high stress and strain  
556 during masticatory loading in humans (Endo, 1965, 1966; Arbel, Hershkovitz & Gross, 2000;  
557 Szwedowski, Fialkov & Whyne, 2011; Maloul et al., 2012). This region is often described as a  
558 pillar-like structure (Benninghoff, 1925; Bluntschili, 1926), or section of a frame-like structure  
559 (Görke, 1902; Endo, 1965, 1966), that resists mainly compression during anterior tooth biting.  
560 The results of our analysis are in general agreement with these findings, except that tension at the  
561 nasal margin was also found to be high in magnitude, indicating intense bending and shearing of  
562 the lower maxillary region during anterior tooth biting (see Fig. 7 and Fig. 9).

563         In addition to the nasal margin, the postorbital bars of the human FEMs were also found  
564 to experience highly elevated von Mises strain magnitudes compared to chimpanzees. However,  
565 adjacent regions, including the zygoma/zygomatic body (“cheek bone”) region and zygomatic  
566 arch, were found to be similar in strength to the lower end of the chimpanzee range. Mechanical  
567 analyses of *Paranthropus boisei* and *Australopithecus africanus* (Smith et al., 2015a) show a  
568 similar pattern of relatively low strains in the zygomatic body. Smith et al. (2015a) suggest that  
569 the structural strength of the zygomatic body in australopiths could be adaptively significant,  
570 offering as one possibility that it serves to reduce strains in the nearby zygomatico-maxillary  
571 suture. In pigs, it has been demonstrated that unfused sutures can fail at relatively modest stress

572 levels (e.g., Popowics & Herring, 2007), so some bony facial regions may serve to shield nearby  
573 sutures from masticatory stresses rather than bone itself (Wang et al., 2012). Among smaller-  
574 faced modern human crania, the zygomatico-maxillary suture may be especially prone to  
575 experiencing relatively large masticatory stresses. In our FEMs, the largest strains in this region  
576 of the mid-face were generated medial to the zygomatico-maxillary suture. The location of these  
577 elevated strain magnitudes corresponds roughly to the location of facial fractures experienced  
578 commonly during physical altercations (Ellis, El-Attar & Moos, 1985). Facial fractures are also  
579 common at the postorbital bar, as opposed to the zygomatic body or zygomatico-maxillary  
580 suture, when the zygomatic body is exposed to traumatic blows (Ellis, 2012; Pollock, 2012).  
581 Therefore, it is possible that the strength of the human zygomatic body, and perhaps the relative  
582 weakness of the postorbital bar, is related to diverting stress from sutures that might otherwise  
583 fail under relatively lower stress magnitudes.

584         In addition to the zygomatic body (“cheek bone”) region, humans were found to exhibit  
585 lower average von Mises strains and markedly lower peak strains than chimpanzees at the mid-  
586 zygomatic arch, although human values were bracketed by the range of chimp values. This  
587 potentially reflects differences in arch length. Specifically, the size of the temporalis muscle,  
588 which is correlated with the area of the infratemporal fossa (Weijjs & Hillen, 1984), is  
589 significantly reduced in humans compared to that of chimpanzees (Taylor & Vinyard, 2013).  
590 Demes & Creel (1988) show that the area of the infratemporal fossa is nearly half that of  
591 chimpanzees, meaning that the total length of the zygomatic arch is also reduced. Bone strain  
592 analyses demonstrate that the arch is subjected to sagittal bending, as well as torsion along its  
593 long axis (e.g., Hylander, Johnson & Picq, 1991; Hylander and Johnson, 1997; Ross, 2001; Ross  
594 et al., 2011). Predictions based on beam theory therefore suggest that a decrease in the length of

595 the arch will lessen these bending and torsional moments, whereas a reduction in the height  
596 and/or breadth of the arch will weaken it under bending and shear, respectively.

597         Functional interpretations based on the morphology of the zygomatic arch are  
598 complicated by the fact that the temporalis fascia has been hypothesized to stabilize it from the  
599 inferiorly-directed pulling action of the masseter muscle (Eisenberg & Brodie, 1965). Curtis et  
600 al. (2011) tested this hypothesis using FEA and found that models that do not include the  
601 temporalis fascia will overestimate strains in the arch and surrounding regions, including the  
602 postorbital bar and infraorbital. However, they also found that their models lacking a fascia  
603 generated strains more similar in magnitude to those collected during *in vivo* experiments  
604 (Hylander, Johnson & Picq, 1991; Hylander and Johnson, 1997; Ross, 2001; Ross et al., 2011).  
605 Similarly, previous FEA studies on primate crania that have not included a modeled fascia (e.g.,  
606 Ross et al., 2005, 2011; Strait et al., 2005) also find broad agreement with *in vivo* data.  
607 Therefore, we did not feel that it was necessary to include this structure in our FEMs.  
608 Importantly, Curtis et al. (2011) did not actually model the temporalis fascia, rather, they applied  
609 external forces along the margin of the attachment of the fascia. This procedure assumes that the  
610 load transferred to bone by the fascia is evenly distributed around its perimeter. However, the  
611 fascia is subjected to load by the inferiorly directed force produced by those temporalis fibers  
612 that arise off of the deep surface of the fascia. This force should elevate tension in the fascia  
613 along its superior margin (i.e., where it arises off of the superior temporal line) while reducing  
614 tension along its inferior margin (i.e., along the arch). This factor may mitigate the role of the  
615 fascia in resisting the contraction of the masseter muscle.

616         Although the brow ridges are not thought to play an important role in masticatory stress  
617 resistance (e.g., Picq & Hylander, 1989; Hylander, Johnson & Picq, 1991; Ravosa, 1991a,b;

618 Ravosa et al., 2000) it is interesting to note that our human FEMs experienced higher von Mises  
619 strain magnitudes than chimpanzees at all three of the supraorbital sites examined, particularly  
620 during premolar biting. Between the human and chimpanzee samples, differences were found to  
621 be greatest at the working and balancing dorsal orbitals, not the dorsal interorbital, supporting the  
622 idea that the brow ridge cannot be modeled as a bent beam (Picq & Hylander, 1989; see also  
623 Chalk et al., 2011). The fact that the smaller brows of humans experienced elevated strain  
624 magnitudes during biting could be interpreted as meaning that large brow ridges are an  
625 adaptation to resist masticatory loads. However, a wealth of experimental data on humans and  
626 non-human primate species has shown (e.g., Hylander, Johnson & Picq, 1991; Ravosa et al.,  
627 2000; Szwedowski, Fialkov & Whyne, 2011; Ross et al., 2011; Maloul et al., 2012) that strains  
628 along the supraorbital margin are relatively low during biting and chewing, which is supported  
629 by the results presented here. Therefore, it is more reasonable to interpret differences in  
630 supraorbital morphology between humans and chimpanzees as being related to some non-dietary  
631 function, and that the resulting increases in brow ridge strain among humans are experienced as a  
632 secondary byproduct. For example, Moss and Young (1966) suggest that a large separation is  
633 formed posterior to the orbits when brain size is small, forming a supraorbital ridge. When brain  
634 size is large, the frontal bone is more steeply inclined posterior to the orbits, forming a vertical  
635 forehead rather than a large torus. A byproduct of this missing bar of bone above the orbits  
636 among modern humans could be that strain magnitudes are mildly elevated in that region.

637 Overall, our findings show that the human craniofacial skeleton is weaker than that of  
638 chimpanzees when subjected to feeding loads. These findings support the hypothesis that dietary  
639 changes involving a shift to softer and/or more processed foods along the modern human lineage  
640 has led to masticatory gracilization and reduced structural strength of the bony facial skeleton

641 (e.g., Lieberman et al., 2004). However, in their biomechanical analysis, Wroe et al. (2010)  
642 recently found that although the human cranium is less robust, it experiences low peak strains  
643 and an even distribution of facial strain magnitudes compared to extant apes and fossil  
644 australopith species. Differences between our results and those of Wroe et al. (2010) could  
645 reflect differences in the way muscle loads were applied to the models in each analysis and/or the  
646 manner in which models were constrained. For example, we applied both normal and tangential  
647 tractions over entire muscle areas using Boneload (Grosse et al., 2007), whereas Wroe et al.  
648 (2010) loaded their models with muscles modeled as straight pre-tensioned beam elements.  
649 However, we conducted a sensitivity analysis to explore this possibility further (see  
650 Supplementary Information) and found that these differences in methodology only resulted in  
651 small differences in strain magnitude at most locations across the craniofacial skeleton.

652 Another possible explanation for the differences between our study and the study by  
653 Wroe et al. (2010) relates to the magnitudes of the applied muscle forces. Wroe et al. (2010)  
654 subjected their FEMs to three sets of simulated biting on various teeth. In their first simulation of  
655 the three, FEMs were assigned a set of species-specific muscle forces (or muscle force estimates)  
656 from the literature. In a second simulation, models were scaled to the surface area of their  
657 chimpanzee model and re-loaded using chimpanzee muscle forces. Lastly, in the third  
658 simulation, models were scaled to the surface area of their chimpanzee model and loaded with  
659 muscle loads required to generate an equivalent bite force. In this third simulation, the high  
660 biting leverage offered by the retracted human face meant that the forces required to generate a  
661 bite compared to the other hominoids examined were relatively low. Therefore, Wroe et al.  
662 (2010) concluded that the human facial skeleton may in fact be well-adapted to resist masticatory  
663 stresses generated during high magnitude biting. Importantly, however, mean element von Mises

664 stresses were found to be relatively high in their human FEM during the second simulation,  
665 where FEMs were scaled to the same surface area and loaded with equivalent muscle forces.  
666 This is the most similar of their three scaling procedures to the scaling performed here (scaling  
667 muscle forces to model volume<sup>2/3</sup>), which we believe is the best means for removing the effects  
668 of size on comparisons of mechanical performance (e.g., Dumont, Grosse & Slater, 2009; Strait  
669 et al., 2010).

670

671 *Bite force production and efficiency: are humans suited to produce large biting forces?*

672         When analyzed using human bone and muscle properties (i.e., ALL-HUM models), our  
673 human FEMs produced bite forces of 333-507 N at the premolar (P<sup>3</sup>) and 496-756 N at the molar  
674 (M<sup>2</sup>). These results are similar to, but lower than, previous estimates of human bite force  
675 production using both 2D and 3D modeling techniques (e.g., Wroe et al., 2010; Eng et al., 2013).  
676 For example, using skeletal measurements and data on muscle cross-section, Eng et al. (2013)  
677 recently estimated that humans are capable of producing approximately 660-1106 N of M<sup>2</sup> bite  
678 force, while Wroe et al. (2010) estimated a maximum unilateral M<sup>2</sup> bite force of 1109-1317 N  
679 using FEA. However, our M<sup>2</sup> bite force results are bracketed by bite force transducer data  
680 collected from various western populations, which range from approximately 368 N (Sinn, de  
681 Assis & Throckmorton, 1996) to around 911 N (Waltimo, Nystram & Kananen 1994), although  
682 Inuit males have been shown to produce an average of 1277 N in M<sup>2</sup> bite force (Waugh, 1937).  
683 Therefore, our results for bite force production lie within and do not exceed the known range of  
684 *in vivo* variation exhibited by recent human populations.

685         Because chimpanzees have absolutely and relatively larger jaw adductor muscles than  
686 humans (e.g., Taylor & Vinyard, 2013), it is no surprise that the chimp FEMs were capable of

687 producing more forceful bites than our human FEMs when loaded with species-specific muscle  
688 forces (compare data in Table 9 to Smith et al., 2015b, Table 4). However, when loaded with  
689 muscle forces scaled to remove differences in size (as in the CHIMPED model variants), we  
690 found that humans are more *efficient* producers of bite forces, in terms of biting leverage,  
691 consistent with the findings of Wroe et al. (2010). Specifically, the mechanical advantage (MA)  
692 for P<sup>3</sup> biting in humans ranged 0.39-0.47, compared to 0.32-0.42 in chimpanzees (Smith et al.,  
693 2015b), with only two chimps overlapping the human range. Humans were found to exhibit even  
694 more elevated leverage during M<sup>2</sup> biting (0.60-0.71), with only one individual overlapping the  
695 chimpanzee range (0.49-0.61). When comparing these data using statistical analysis as a  
696 heuristic guide, humans were found to be significantly more efficient at producing bite forces at  
697 both mesial and distal bite points. The CHIMPED humans were even found to exhibit a biting  
698 efficiency similar to that observed in australopiths (Smith et al., 2015a). In fact, P<sup>3</sup> MA in *P.*  
699 *boisei* (0.40) and *A. africanus* (0.41) were near the lower end observed in humans. The FEM of  
700 *A. africanus* also generated M<sup>2</sup> bites with similar efficiency (0.62) to humans, whereas *P. boisei*  
701 produced more mechanically efficient (0.75) molar bites (Smith et al., 2015a).

702         Our data on bite force efficiency in humans support previous findings that have  
703 demonstrated the mechanical advantage of modern human bony facial architecture compared to  
704 both non-modern humans and non-human primate species (e.g., Spencer & Demes, 1993;  
705 O'Connor, Franciscus & Holton, 2005; Lieberman, 2008, 2011; Wroe et al., 2010; Eng et al.,  
706 2013). Using estimates of muscle leverage from 2D measurements (Lieberman, 2008, 2011),  
707 humans have been shown to achieve high biting leverage through a marked degree of facial  
708 retraction (orthognathism), which reorients the muscles of mastication relative to the tooth rows.  
709 As noted above, we found that our human FEMs produced bite forces with leverage ratios

710 similar to those observed in *A. africanus* and *P. boisei* (Smith et al., 2015a). However,  
711 australopiths achieve high biting leverage through an anterior positioning of the chewing muscles  
712 relative to the tooth rows (Rak, 1983; Strait et al., 2009, 2010; Smith et al., 2015a). In humans,  
713 the midfacial region is “tucked” beneath the anterior cranial fossa (Lieberman, McBratney &  
714 Krovitz, 2002; Lieberman et al., 2004; Lieberman, 2008, 2011), which similarly places bite  
715 points in a position that offers higher mechanical advantage to the jaw adductors.

716         Although the human cranium can theoretically produce mechanically efficient bite forces,  
717 the production of unilateral molar ( $M^2$ ) bite force is limited by the risk of temporomandibular  
718 joint (TMJ) distraction, as predicted by the constrained lever model (Greaves, 1978; Spencer,  
719 1998, 1999). Specifically, we found that all seven of the CHIMPED human FEMs experienced a  
720 highly distractive (tensile) reaction force at the working-side joint during molar biting. These  
721 forces have the effect of “pulling” the mandibular condyle from the jaw joint, increasing the risk  
722 of joint dislocation (Spencer, 1998, 1999). As noted in the introduction, the soft tissues of the  
723 mammalian jaw joint are well suited to resist compressive joint reaction forces, but are poorly  
724 configured to resist distractive joint forces that “pull” the mandibular condyle from the cranial  
725 base (Greaves, 1978; Spencer, 1998, 1999). In contrast, only one of the six chimpanzee FEMs  
726 analyzed by Smith et al. (2015a) generated a tensile force at the working TMJ, and this reaction  
727 was only very weakly tensile (12.7 N). Similarly, Smith et al. (2015b) found that their FEMs of  
728 *P. boisei* and *A. africanus* lacked working-side distraction and were able to produce “stable”  
729 bites on both the premolars and molars, offering these species the ability to produce maximally  
730 forceful molar bites with limited risk of causing pain and/or damage to the TMJ capsule.

731         Interestingly, when loaded with human muscle forces (i.e., ALL-HUM), two of the  
732 human FEMs (TIGA and WAFR) were capable of maintaining weakly compressive reaction



733 forces at both TMJs during molar biting. Additionally, balancing side force reductions required  
734 to eliminate distraction in the remaining models were proportionately less (5-15%) than when  
735 applying chimpanzee forces (15%-30%). Comparisons of the muscle loads applied to the models  
736 and their force ratios in the ALL-HUM and CHIMPED models (see Tables 9 and 11) reveal that  
737 chimpanzees devote a higher proportion of muscle strength to anteriorly-positioned muscle  
738 compartments (superficial masseter and anterior temporalis) compared to more posteriorly-  
739 positioned ones (deep masseter and medial pterygoid). Therefore, it is tempting to suggest that  
740 changes in human jaw muscle force ratios may have coincided with the retraction of the lower  
741 face during human evolution in order to reduce the risk of TMJ distraction. Likewise, if the  
742 repositioning of cranial elements for reasons other than food processing (Lieberman, 2008;  
743 Lieberman & Zink, 2016) led to an increase in biting efficiency but the generation of working  
744 side joint distraction during molar biting, the overall reduction of chewing muscle size in *Homo*  
745 could also be viewed as a result of positive selection rather than relaxed selection so as to lessen  
746 these distractive forces.

747         Our findings that humans are limited in their ability to produce forceful unilateral molar  
748 bites are supported by data on bite force and muscle activity in humans. Spencer (1995, 1998)  
749 tested some predictions of the constrained lever model and found that humans produced bite  
750 forces that increased as the bite point moved from the incisors to the first molar. Moving from  
751  $M^1$  to  $M^3$ , bite forces were found to decrease as a result of the decreasing balancing force muscle  
752 recruitment required to avoid joint distraction. Spencer (1995) also notes that most of the  
753 participants (8 of 10) in his analysis reported pain near the working-side TMJ when biting  
754 forcefully using the back molars. In addition to this study, Hylander (1977) suggests that  
755 specialized anterior tooth biting and increased masticatory muscle leverage may be related to the

756 high incidence of third molar reduction and agenesis among modern Inuit due to the increased  
757 risk of distraction when biting on these teeth, although the results of our single pre-historic  
758 Arctic FEM (TIGA) provide no support for this hypothesis. Similarly, Spencer (2003)  
759 demonstrates that seed predating New World primates with adaptations for increased anterior  
760 bite force have relatively small third molar roots.

761 As discussed above, Wroe et al. (2010) analyzed human feeding biomechanics within a  
762 comparative context. One of the principal findings of their analysis, supported by the data  
763 presented here, is that humans are capable of generating bite forces with higher mechanical  
764 efficiency than chimpanzees. Wroe et al. use this as evidence to argue that human craniofacial  
765 evolution may have been influenced by selection for powerful biting behaviors. However, the  
766 results of this study showing the comparative weakness of the human cranium combined with the  
767 increased risk of jaw joint distraction during molar biting leads us to interpret the increased  
768 biting leverage exhibited by humans, which is particularly high among recent populations  
769 (Spencer & Demes, 1993; O'Connor, Franciscus & Holton, 2005), to be a byproduct of human  
770 facial orthognathism, which may be at least partly related to facial size reduction. Human facial  
771 flatness may also have been acquired through selection for some non-dietary function. For  
772 example, Lieberman (2008, 2011) suggests that the marked degree of facial retraction exhibited  
773 by modern human crania could be related to changes in brain size and cranial base flexion.  
774 However, Ross (2013) shows that basicranial flexion cannot produce significant facial retraction  
775 on its own. Alternatively, Holton et al. (2010) propose that dietary shifts leading to reduced  
776 facial strain magnitudes among early human species may have led to reduced facial growth and  
777 earlier fusion of the maxillary sutures, and thus smaller and more retracted facial skeletons.

778           Although the majority of the morphological and mechanical evidence is not consistent  
779 with the hypothesis that the human masticatory apparatus has experienced recent *selection* for  
780 high magnitude biting, the results of our analysis cannot reject the hypothesis that, in addition to  
781 changes in diet and tool use, increases in muscle force efficiency during human evolution could  
782 have led to relaxed selection for large chewing muscle size and reductions in facial size (Wroe et  
783 al., 2010) or that humans benefited from increased biting leverage when using submaximal  
784 forces by exerting less energy per bite. Our results for premolar biting leverage also do not  
785 conflict directly with the hypothesis that anterior tooth biting could have been selectively  
786 important in humans. However, the reduced size of the premolar teeth in humans increases the  
787 risk of tooth crown fracture (Constantino et al., 2010). Therefore, studies on premolar size and  
788 strength are not consistent with the hypothesis that humans are particularly well adapted for  
789 forcefully loading their anterior teeth, but such studies have yet to be conducted on incisors or  
790 canines, which are the more likely to be used during paramasticatory activities. For example,  
791 Hylander (1977) identifies features of the modern Inuit craniofacial skeleton that he argues to be  
792 adaptations for powerful biting behaviors using the incisors, although our single pre-historic  
793 Arctic FEM (TIGA) was not found to be exceptional in this regard. Additionally, Spencer &  
794 Ungar (2000) show that incisor bite force leverage varies in relation to the intensity of incisor  
795 tooth use among some Native American populations. Similarly, it is possible that differences in  
796 anterior tooth use among “archaic” members of the genus *Homo* are reflected in mechanical  
797 differences between the species. In particular, the Neanderthals (*H. neanderthalensis*) exhibit a  
798 number of derived characteristics hypothesized to be adaptations for forceful incisor biting (e.g.,  
799 Brace, 1962; Smith, 1983; Trinkaus, 1983, 1987; Rak, 1986; Demes, 1987). Notably, Spencer &  
800 Demes (1993) show that Neanderthals exhibit high incisor bite force leverage relative to *H.*

801 *heidelbergensis* (but not modern *H. sapiens*). In order to maintain functional use of the posterior  
802 dentition (i.e., avoid TMJ distraction), Spencer & Demes (1993) further show that the molar  
803 tooth row in Neanderthals was anteriorly shifted, resulting in the characteristic retromolar gap.

804 Data on enamel thickness seemingly contrasts with the hypothesis that humans have  
805 experienced relaxed selection for powerful biting behaviors. Specifically, a number of studies  
806 find that recent human populations exhibit thick molar enamel (e.g., Martin, 1983, 1985;  
807 Olejniczak et al., 2008; Smith et al., 2006; Vogel et al., 2008), which has been interpreted as a  
808 primitive retention. However, notwithstanding disagreements over the significance of enamel  
809 thickness (Grine, 2005), Smith et al. (2012) recently show that “thick” molar enamel in humans  
810 is primarily the result of small coronal dentine areas. They found that enamel area in humans is  
811 reduced, but there was a disproportionately large reduction in dentine to enamel as human teeth  
812 were evolving smaller size, resulting in a relatively “thick” enamel cap. Thus, Smith et al. (2012)  
813 argue that the dichotomy between thick and thin enamel is an oversimplification.

814

## 815 CONCLUSIONS

816 We examined the biomechanical consequences of human masticatory gracilization and  
817 intraspecific variation within the constrained lever model of feeding biomechanics (Spencer,  
818 1999) and tested the hypothesis that the human face is well configured to *generate* and *withstand*  
819 high biting forces relative to chimpanzees. We found that our biomechanical models of human  
820 crania were, on average, less structurally stiff than the crania of chimpanzees when assigned  
821 equivalent bone properties, constraints, and physiologically-scaled muscle forces. These results  
822 are consistent with the facial reduction exhibited by modern humans. We also found that modern  
823 humans are efficient producers of bite force, consistent with previous analyses (Spencer &

824 Demes, 1993; O'Connor, Franciscus & Holton, 2005; Lieberman, 2008, 2011; Wroe et al., 2010;  
825 Eng et al., 2013), but that distractive (tensile) reaction forces are generated at the working  
826 (biting) side jaw joint during M<sup>2</sup> biting. In life, such a configuration would have increased the  
827 risk of joint dislocation and constrained the maximum recruitment levels of the masticatory  
828 muscles, meaning that the human cranium is poorly suited to produce forceful unilateral molar  
829 bites. Our results do not conflict directly with the hypothesis that premolar biting could have  
830 been selectively important in humans, although the reduced size of these teeth in humans has  
831 been shown to increase the risk of tooth crown fracture. We interpret our results to suggest that  
832 human craniofacial evolution was probably not driven by selection for high magnitude biting,  
833 and that increased masticatory muscle efficiency in humans is likely to be a byproduct of  
834 selection for some non-dietary function (Lieberman, 2008) or perhaps related to reduced  
835 masticatory strain and sutural growth restrictions (Holton et al., 2010).

836         Our results provide support for the hypothesis that a shift to the consumption of less  
837 mechanically challenging foods and/or the innovation of extra-oral food processing techniques  
838 (e.g., stone tool use, cooking) along the lineage leading to modern *Homo sapiens* relaxed the  
839 selective pressures maintaining features favoring forceful biting and chewing behaviors,  
840 including large teeth and robust facial skeletons, leading to the characteristically small and  
841 gracile faces of modern humans (e.g., Brace, Smith & Hunt, 1991; Wrangham et al., 1999;  
842 Lieberman et al., 2004; Ungar et al., 2006a,b; Wood, 2009). To contribute to our further  
843 understanding, future studies should aim to identify the ecological changes that may have led to  
844 the emergence of such shifts in dietary behavior. Were these changes initiated by changes in  
845 climate, competition, resource availability, or some combination of these factors? To what extent  
846 is craniofacial gracilization part of a general pattern of skeletal gracilization in humans (Ruff et

847 al, 1993, 2015; Chirchir et al, 2015; Ryan & Shaw, 2015)? These questions will be addressed by  
848 gaining further insight into the dietary ecology and feeding adaptations of species near the  
849 origins of the modern human lineage through work on biomechanics, paleoecology, archaeology,  
850 bone chemistry, and dental wear, each of which inform key components necessary to obtaining a  
851 more complete understanding of human craniofacial evolution.

852

### 853 **ACKNOWLEDGEMENTS**

854 We thank Gisselle Garcia-Pack and Kristen Mable of the AMNH for access to human skeletal  
855 collections. We also thank Tim Ryan and Tim Stecko of the Center for Quantitative Imaging at  
856 Penn State for assistance in acquiring CT image data of modern human crania.

857

### 858 **REFERENCES**

- 859 Agrawal KR, Lucas PW, Prinz JF, Bruce IC. 1997. Mechanical properties of foods responsible  
860 for resisting food breakdown in the human mouth. *Arch Oral Biol* 42:1-9.
- 861 Arbel G, Hershkovitz I, Gross MD. 2000. Strain distribution on the skull due to occlusal loading:  
862 an anthropological perspective. *Homo* 51:30-55.
- 863 Baab KL, Freidline SE, Wang SL, Hanson T. 2010. Relationship of cranial robusticity to cranial  
864 form, geography and climate in *Homo sapiens*. *Am J Phys Anthropol* 141:97-115.
- 865 Benninghoff A. 1925. Spaltlinien am Knochen, ein method zur ermittlung der architektur platter  
866 kochen. *Verh Anat Ges* 34:189-206.
- 867 Berger LR, de Ruiter DJ, Churchill SE, Schmid P, Carlson KJ, Dirks PHGM, Kibii JM. 2010.  
868 *Australopithecus sediba*: a new species of *Homo*-like australopith from South Africa.  
869 *Science* 328:195-204.

- 870 Bluntschli H. 1926. Rückwirkung des Kieferapparates auf den Gesamtschädel. *Z zahnärztl*  
871 *Orthopäd* 18:57-59.
- 872 Bookstein FL. 1991. *Morphometric tools for landmark data: geometry and biology*. Cambridge:  
873 Cambridge University Press.
- 874 Brace CL. 1962. Cultural factors in the evolution of the human dentition. In: Montague MFA,  
875 editor. *Culture and the evolution of man*. Oxford: Oxford University Press. p 343-354.
- 876 Brace C, Smith SL, Hunt KD. 1991. What big teeth you had grandma! Human tooth size, past  
877 and present. *Advances in Dental Anthropology* 33-57.
- 878 Carmody RN, Wrangham RW. 2009. The energetic significance of cooking. *J Hum Evol* 57:379-  
879 391.
- 880 Carmody RN, Weintraub GS, Wrangham RW. 2011. Energetic consequences of thermal and  
881 nonthermal food processing. *Proc Natl Acad Sci USA* 108:19199-19203.
- 882 Chalk J, Richmond BG, Ross CF, Strait DS, Wright BW, Spencer MA, Wang Q, Dechow PC.  
883 2011. A finite element analysis of masticatory stress hypotheses. *Am J Phys Anthropol*.  
884 145:1-10.
- 885 Chirchir H, Kivell TL, Ruff CB, Hublin J-J, Carlson K, Zipfel B, Richmond BG. 2015. Recent  
886 origin of low trabecular bone density in modern humans. *Proc Natl Acad Sci USA*  
887 112:366-371.
- 888 Constantino PJ, Lee JJ-W, Chai H, Zipfel B, Ziscoveri C, Lawn BR, Lucas PW. 2010. Tooth  
889 chipping can reveal the diet and bite forces of fossil hominins. *Biol Lett* 6:826-829.
- 890 Curtis N, Witzel U, Fitton L, O'Higgins P, Fagan M. 2011. The mechanical significance of the  
891 temporal fasciae in *Macaca fascicularis*: an investigation using finite element analysis.
- 892 Davis JL, Dumont ER, Strait DS, Grosse IR. 2011. An efficient method of modeling

- 893 material properties using a thermal diffusion analogy: an example based on  
894 craniofacial bone. PLoS ONE 6:e17004.
- 895 Demes B. 1987. Another look at an old face: biomechanics of the neandertal facial skeleton  
896 reconsidered. J Hum Evol 16:297-303.
- 897 Demes B, Creel N. 1988. Bite force, diet, and cranial morphology of fossil hominids. J Hum  
898 Evol 17:657-670.
- 899 Dumont ER, Grosse IR, Slater GJ. 2009. Requirements for comparing the performance of  
900 finite element models of biological structures. J Theor Biol 256:96-103.
- 901 Eisenberg NA, Brodie AG. 1965. Antagonism of temporal fascia to masseteric contraction. Anat  
902 Rec 152:185-192.
- 903 Ellis E, El-Attar A, Moos KF. 1985. An analysis of 2,067 cases of zygomatico-orbital fracture. J  
904 Oral Maxillofac Surg 43:417-428.
- 905 Ellis E. 2012. Chapter 16: Fractures of the zygomatic complex and arch. In: Fonseca RJ, Barber  
906 HD, Powers MP, Frost DE, editors. Oral and Maxillofacial Trauma. St. Louis, MO:  
907 Saunders. p 354-415.
- 908 Endo B. 1965. Distribution of stress and strain produced in the human facial skeleton by  
909 masticatory force. J Anthropol Soc Nippon 73:123-136.
- 910 Endo B. 1966. Experimental studies on the mechanical significance of the form of the human  
911 facial skeleton. J Faculty of Sci 3:1-106.
- 912 Eng CM, Lieberman DE, Zink KD, Peters MA. 2013. Bite force and occlusal stress production in  
913 hominin evolution. Am J Phys Anthropol 151:544-557.
- 914 Fleagle JG, Gilbert CC, Baden AL. 2010. Primate cranial diversity. Am J Phys Anthropol  
915 142:565-578.



- 916 Görke O. 1904. Beitrag zur funktionellen gestaltung des schadels bei den anthropomorphen und  
917 menschen durch untersuchung mit rontgenstrahlen. Arch Anthropol 1:91-108.
- 918 Greaves WS. 1978. The jaw lever system in ungulates: a new model. J Zool 184:271-285.
- 919 Grine FE. 2005. Enamel thickness of deciduous and permanent molars in modern *Homo sapiens*.  
920 Am J Phys Anthropol. 126:14-31.
- 921 Groopman EE, Carmody RN, Wrangham RW. 2015. Cooking increases net energy gain from a  
922 lipid-rich food. AM J Phys Anthropol 156:11-18.
- 923 Grosse IR, Dumont ER, Coletta C, Tolleson A. 2007. Techniques for modeling muscle  
924 induced forces in finite element models of skeletal structures. Anat Rec 290A:1069-1088.
- 925 Holton NE, Franciscus RG, Nieves MA, Marshall SD, Reimer SB, Southard, TE, Keller JC,  
926 Maddux SD. 2010. Sutural growth restriction and modern human facial evolution: an  
927 experimental study in a pig model. J Anat 216:48-61.
- 928 Hylander WL. 1977. The adaptive significance of Eskimo craniofacial morphology. In: Dahlberg  
929 AA, Graber TM, editors. Orofacial growth and development. Chicago, IL: Aldine  
930 Publishing Company. p 129-169.
- 931 Hylander WL, Johnson KR. 1997. *In vivo* bone strain patterns in the zygomatic arch of macaques  
932 and the significance of these patterns for functional interpretations of craniofacial form.  
933 Am J Phys Anthropol 102:203-232.
- 934 Hylander WL, Johnson KR, Picq PG. 1991. Masticatory-stress hypotheses and the supraorbital  
935 region of primates. Am J Phys Anthropol 86:1-36.
- 936 Keyak JH, Rossi SA. 2000. Prediction of femoral fracture load using finite element models: an  
937 examination of stress- and strain-based failure theories. J Biomech 33:209-214.
- 938 Kimbel WH, Rak Y, Johanson DC. 2004. The skull of *Australopithecus afarensis*. New York:

- 939 Oxford University Press.
- 940 Ledogar JA. 2015. Human feeding biomechanics: intraspecific variation and evolution. Ph.D  
941 dissertation, University at Albany.
- 942 Lieberman DE. 2008. Speculations about the selective basis for modern human craniofacial  
943 form. *Evol Anthropol* 17:55-68.
- 944 Lieberman DE. 2011. The evolution of the human head. Cambridge, MA: Belknap Press.
- 945 Lieberman DE, McBratney BM, Krovitz GE. 2002. The evolution and development of cranial  
946 form in *Homo sapiens*. *Proc Natl Acad Sci USA* 99:1134-1139.
- 947 Lieberman DE, Krovitz G, Devlin M, Yates F, St. Clair M. 2004. Effects of food processing on  
948 masticatory strain and craniofacial growth in a retrognathic face. *J Hum Evol* 46:655-677.
- 949 Lucas PW. 2004. Dental function morphology: how teeth work. Cambridge: Cambridge  
950 University Press.
- 951 Lucas PW, Luke DA. 1984. Optimum mouthful for food comminution in human mastication.  
952 *Arch Oral Biol* 29:205-210.
- 953 Maloul A, Fialkov J, Whyne C. 2011. The impact of voxel size-based inaccuracies on the  
954 mechanical behavior of thin bone structures. *Ann Biomed Eng* 39:1092-1100.
- 955 Maloul A, Regev E, Whyne CM, Beek M, Fialkov JA. 2012. *In vitro* quantification of strain  
956 patterns in the craniofacial skeleton due to masseter and temporalis activities. *J Craniofac  
957 Surg* 23:1529-1534.
- 958 Martin LB. 1983. Relationships of the later Miocene Hominoidea. Ph.D dissertation,  
959 University College London.
- 960 Martin LB. 1985. Significance of enamel thickness in hominoid evolution. *Nature* 314:260-263.
- 961 Moss ML, Young RW. 1960. A functional approach to craniology. *Am J Phys Anthropol*

- 962 18:281-292.
- 963 Mundry R, Fischer J. 1998. Use of statistical programs for nonparametric tests of small samples  
964 often leads to incorrect p-values: examples from animal behavior. *Anim Behav* 56:256-  
965 259.
- 966 Murphy RA. 1998. Skeletal muscle. In: Berne RM, Levy MN, editors. *Physiology*. St. Louis,  
967 MO: Mosby. p 294.
- 968 Nagasao T, Nakajima T, Kimura A, Kaneko T, Jin H, Tamaki T. 2005. The dynamic role of  
969 buttress reconstruction after maxillectomy. *Plast Reconstr Surg* 115:1138-1349.
- 970 O'Connor CF, Franciscus RG, Holton NE. 2005. Bite force production capability and efficiency  
971 in neandertals and modern humans. *Am J Phys Anthropol* 127:129-151.
- 972 Olejniczak AJ, Smith TM, Feeney RN, Macchiarelli R, Mazurier A, Bondioli L, Rosas A, Fortea  
973 J, del la Rasilla M, Garcia-Taberner A, Radovic J, Skinner MM, Toussaint M, Hublin  
974 J-J. 2008. Dental tissue proportions and enamel thickness in Neandertal and modern  
975 human molars. *J Hum Evol* 55:12-23.
- 976 Organ C, Nunn CL, Machanda Z, Wrangham RW. 2011. Phylogenetic rate shifts in feeding time  
977 during the evolution of *Homo*. *Proc Natl Acad Sci USA* 108:14555-14559.
- 978 Peterson J, Dechow PC. 2002. Material properties of the inner and outer cortical tables of the  
979 human parietal bone. *Anat Rec* 268:7-15.
- 980 Picq PG, Hylander WL. 1989. Endo's stress analysis of the primate skull and the functional  
981 significance of the supraorbital region. *Am J Phys Anthropol* 79:393-398.
- 982 Pollock RA. 2012. *Craniomaxillofacial buttresses: anatomy and operative repair*. New York:  
983 Thieme Medical Publishers.

- 984 Popowics TE, Herring SW. 2007. Load transmission in the nasofrontal suture of the pig, *Sus*  
985 *scrofa*. J Biomech 40:837–844.
- 986 Rak Y. 1983. The australopithecine face. New York: Academic Press.
- 987 Rak Y. 1986. The Neanderthal face: a new look at an old face. J Hum Evol 15:151-164.
- 988 Ravosa MJ. 1991a. Ontogenetic perspective on mechanical and non-mechanical models of  
989 primate circumorbital morphology. Am J Phys Anthropol 85: 95-112.
- 990 Ravosa MJ. 1991b. Interspecific perspective on mechanical and nonmechanical models of  
991 primate circumorbital morphology. Am J Phys Anthropol 86: 369-396.
- 992 Ravosa MJ, Noble VE, Hylander WL, Johnson KR, Kowalski EM. 2000. Masticatory stress,  
993 orbital orientation and the evolution of the primate postorbital bar. J Hum Evol 38:667-  
994 693.
- 995 Robinson JT. 1954. Prehominid dentition and hominid evolution. Evolution (N Y) 8:325-334.
- 996 Ross CF. 2001. *In vivo* function of the craniofacial haft: the interorbital “pillar.” Am J Phys  
997 Anthropol 116:108-139.
- 998 Ross CF. 2013. Complexity, modularity, and integration in the human head. J Hum Evol 64:56-  
999 67.
- 1000 Ross CF, Iriarte-Diaz J. 2014. What does feeding system morphology tell us about feeding? Evol  
1001 Anthropol 23:105-120.
- 1002 Ross CF, Patel BA, Slice DE, Strait DS, Dechow PC, Richmond BG, Spencer MA. 2005.  
1003 Modeling masticatory muscle force in finite-element analysis: sensitivity analysis using  
1004 principal coordinates analysis. Ant Rec 283A:288-299.
- 1005 Ross CF, Berthaume MA, Dechow PC, Iriarte-Diaz J, Porro LB, Richmond BG, Spencer M,  
1006 Strait DS. 2011. *In vivo* bone strain and finite-element modeling of the craniofacial haft

- 1007           in catarrhine primates. *J Anat* 218:112-141.
- 1008 Ruff CB, Trinkaus E, Walker AC, Larsen CS. 1993. Postcranial robusticity in *Homo*. I:  
1009 Temporal  
1010 trends and mechanical interpretation. *Am J Phys Anthropol.* 91: 21-53.
- 1011 Ruff CB, Holt B, Niskanen M, Sladek V, Berner M, Garofalo E, Garvin HM, Hora M, Junno J-  
1012 A,  
1013 Schuplerova E, Vilkkama R, Whitty E. 2015. Gradual decline in mobility with the  
1014 adoption of food production in Europe. *Proc Natl Acad Sci USA* 112:7147-7152.
- 1015 Ryan TM, Shaw CN. 2015. Gracility of the modern *Homo sapiens* skeleton is the result of  
1016 decreased biomechanical loading. *Proc Natl Acad Sci USA* 112:372-377.
- 1017 Schwartz-Dabney CL, Dechow PC. 2002. Accuracy of elastic property measurement in  
1018 mandibular cortical bone is improved by using cylindrical specimens. *J Biomech*  
1019 *Eng* 124:714-723.
- 1020 Sinn DP, de Assis EA, Throckmorton GS. 1996. Mandibular excursions and maximum bite  
1021 forces in patients with temporomandibular joint disorders. *J Oral Maxillofac Surg*  
1022 54:671-679.
- 1023 Skelton RR, McHenry HM. 1992. Evolutionary relationships among early hominids. *J Hum Evol*  
1024 23:309-349.
- 1025 Slice DE, ed. 2005. *Modern morphometrics in physical anthropology*, vol. 6. Springer Science &  
1026 Business Media.
- 1027 Smith FH. 1983. Behavioral interpretations of changes in craniofacial morphology across the  
1028 archaic/modern *Homo sapiens* transition. In. Trinkaus E, editor. *The Mousterian legacy*.  
1029 BAR. p. 141-163.

- 1030 Smith AL, Benazzi S, Ledogar JA, Tamvada K, Pryor Smith LC, Weber GW, Spencer MA,  
1031 Lucas PW, Michael S, Shekeban A, Al-Fadhalah K, Almusallam AS, Dechow PC,  
1032 Groasse IR, Ross CF, Madden RH, Richmond BG, Wright BW, Wang Q, Byron C, Slice  
1033 DE, Wood S, Dzialo C, Berthaume MA, van Casteren A, Strait DS. 2015a. The feeding  
1034 biomechanics and dietary ecology of *Paranthropus boisei*. *Ant Rec* 298:145-167.
- 1035 Smith AL, Benazzi S, Ledogar JA, Tamvada K, Pryor Smith LC, Weber GW, Spencer MA,  
1036 Dechow PC, Grosse IR, Ross CF, Richmond BG, Wright BW, Wang Q, Byron C, Slice  
1037 DE, Strait DS. 2015b. Biomechanical implications of intraspecific shape variation in  
1038 chimpanzee crania: moving towards an integration of geometric morphometrics and finite  
1039 element analysis. *Anat Rec* 298:122-144.
- 1040 Smith TM, Olejniczak AJ, Reid DJ, Ferrell RJ, Hublin JJ. 2006. Modern human molar enamel  
1041 thickness and enamel-dentine junction shape. *Arch Oral Biol* 51:974-995.
- 1042 Smith TM, Olejniczak AJ, Zermeno JP, Tafforeau P, Skinner MM, Hoffman A, Radovicic J,  
1043 Toussaint M, Kruszynski R, Menter C, Moggi-Cecchi J, Glasmacher UA, Kullmer O,  
1044 Schrenk F, Stringer C, Hublin J-J. 2012. Variation in enamel thickness within the genus  
1045 *Homo*. *J Hum Evol* 62:395-411.
- 1046 Spencer MA. 1998. Force production in the primate masticatory system: electromyographic  
1047 tests of biomechanical hypotheses. *J Hum Evol* 34:25-54.
- 1048 Spencer MA. 1999. Constraints on masticatory system evolution in anthropoid primates. *Am*  
1049 *J Phys Anthropol* 108:483-506.
- 1050 Spencer MA, Demes B. 1993. Biomechanical analysis of masticatory system configuration in  
1051 Neandertals and Inuits. *Am J Phys Anthropol* 91:1-20.
- 1052 Spencer MA, Ungar PS. 2000. Craniofacial morphology, diet and incisor use in three native

- 1053 American populations. *Inter J Osteoarchaeol* 10:229-241.
- 1054 Spencer MA. 2003. Tooth-root form and function in platyrrhine seed-eaters. *Am J Phys*  
1055 *Anthropol* 122:325-335.
- 1056 Strait DS, Grine FE. 2004. Inferring hominoid and early hominid phylogeny using craniodental  
1057 characters: the role of fossil taxa. *J Hum Evol* 47:399-452.
- 1058 Strait DS, Grine FE, Moniz MA. 1997. A reappraisal of early hominid phylogeny. *J Hum Evol*  
1059 32:17-82.
- 1060 Strait DS, Wang O, Dechow PC, Ross CF, Richmond BG, Spencer MA, Patel BA. 2005.  
1061 Modeling elastic properties in finite element analysis: how much precision is needed to  
1062 produce and accurate model? *Anat Rec* 283A:275-287.
- 1063 Strait DS, Weber GW, Neubauer S, Chalk J, Richmond BG, Lucas PW, Spencer MA,  
1064 Schrein C, Dechow PC, Ross CF, Grosse IR, Wright BW, Constantino P, Wood BA,  
1065 Lawn B, Hylander WL, Wang Q, Byron C, Slice DE, Smith AL. 2009. The feeding  
1066 biomechanics and dietary ecology of *Australopithecus africanus*. *Proc Natl Acad Sci*  
1067 USA 106:2124-2129.
- 1068 Strait DS, Grosse IR, Dechow PC, Smith AL, Wang QW, Weber GW, Neubauer S, Slice DE,  
1069 Chalk J, Richmond BG, Lucas PW, Spencer MA, Schrein C, Wright BW, Byron C, Ross  
1070 CF. 2010. The structural rigidity of the cranium of *Australopithecus africanus*:  
1071 implications for diet, dietary adaptations, and the allometry of feeding biomechanics.  
1072 *Anat Rec* 298:583–593.
- 1073 Strait DS, Constantino P, Lucas PW, Richmond BG, Spencer MA, Dechow PC, Ross  
1074 CF, Grosse IR, Wright BW, Wood BA, Weber GW, Wang Q, Byron C, Slice DE, Chalk  
1075 J, Smith AL, Smith LC, Wood S, Berthaume M, Benazzi S, Dzialo C, Tamvada K,

- 1076 Ledogar JA. 2013. Diet and dietary adaptations in early hominins: the hard food  
1077 perspective. *Am J Phys Anthropol* 151:339-355.
- 1078 Szwedowski TD, Fialkov F, Whyne CM. 2011. Sensitivity analysis of a validated subject-  
1079 specific finite element model of the human craniofacial skeleton. *Proc Inst Mech Eng H*  
1080 225:58-67.
- 1081 Taylor AB, Vinyard CJ. 2013. The relationships among jaw-muscle fiber architecture, jaw  
1082 morphology, and feeding behavior in extant apes and modern humans. *Am J Phys*  
1083 *Anthropol* 151:120-134.
- 1084 Toro-Ibacache V, Zapata Muñoz V, O'Higgins P. 2015. The relationship between skull  
1085 morphology, masticatory muscle force and cranial skeletal deformation during biting.
- 1086 Toro-Ibacache V, Fitton LC, Fagan MJ, O'Higgins P. 2015. Validity and sensitivity of a human  
1087 cranial finite element model: implications for comparative studies of biting performance.
- 1088 Trinkaus E. 1983. Neanderthal postcrania and the adaptive shift to modern humans. In: *The*  
1089 *Mousterian legacy: human biocultural change in the Upper Pleistocene.* p 165-200.  
1090 BAR.
- 1091 Trinkaus E. 1987. The Neandertal face: evolutionary and functional perspectives on a recent  
1092 hominid face. *J Hum Evol* 16:429-443.
- 1093 Ungar P. 2012. Dental evidence for the reconstruction of diet in African early *Homo*. *Curr*  
1094 *Anthropol* 53 S318-S329.
- 1095 Ungar PS, Grine FE, Teaford MF. 2006. Diet in early *Homo*: a review of the evidence and a  
1096 new model of adaptive versatility. *Ann Rev Anthropol* 35:209-228.
- 1097 van Eijden TMGJ, Korfage JAM, Brugman P. 1997. Architecture of the human jaw-closing and  
1098 jaw-opening muscles. *Anat Rec* 248:464-474.



- 1099 Vogel ER, van Woerden JT, Lucas PW, Atmoko SSU, van Schaik CP, Dominy NJ. 2008.  
1100 Functional ecology and evolution of hominoid molar enamel thickness: *Pan troglodytes*  
1101 *schweinfurthii* and *Pongo pygmaeus wurmbii*. J Hum evol 55:60-74.
- 1102 Walker AC. 1991. The origin of genus *Homo*. In: Osawa S, Honjo T, editors. Evolution of Life:  
1103 Fossils, Molecules, and Culture. Tokyo: Springer-Verlag. p 379-389.
- 1104 Waltimo A, Nystram M, Kananen M. 1994. Bite force and dentofacial morphology in men with  
1105 severe dental attrition. E J Oral Sci 102:92-96.
- 1106 Wang Q, Dechow PC. 2006. Elastic properties of external cortical bone in the craniofacial  
1107 skeleton of the rhesus monkey. Am J Phys Anthropol 131:402-415.
- 1108 Wang Q, Strait DS, Dechow PC. 2006. A comparison of cortical elastic properties in the  
1109 craniofacial skeletons of three primate species and its relevance to human evolution. J  
1110 Hum Evol 51:375-382.
- 1111 Wang Q, Wood SA, Grosse IR, Ross CF, Zapata U, Byron CD, Wright BW, Strait DS. 2012.  
1112 The  
1113 role of sutures in biomechanical dynamic simulation of a macaque cranial finite  
1114 element model: implications for the evolution of craniofacial form. Anat Rec  
1115 295:278-288.
- 1116 Waugh L. 1937. Dental observations among Eskimos. J Dent Res 16:355-356.
- 1117 Weijs WA, Hillen B. 1984. Relationships between masticatory muscle cross-section and skull  
1118 shape. J Dent Res 63:1154-1157.
- 1119 Wood BA. 1992. Origin and early evolution of genus *Homo*. Nature 355:783-790.

- 1120 Wood BA. 2009. “Where does the genus *Homo* begin, and how would we know?” The first  
1121 humans: origins of the genus *Homo*. In: Grine FE, Fleagle JG, Leakey RE, editors. New  
1122 York: Springer. p 17-28.
- 1123 Wrangham RW. 2009. *Catching fire: how cooking made us human*. New York: Basic Books.
- 1124 Wrangham RW, Jones JH, Laden G, Pilbeam D, Conklin-Brittain N. 1999. The raw and the  
1125 stolen: cooking and the ecology of human origins. *Curr Anthropol* 40:567-594.
- 1126 Wroe S, Ferrara TL, McHenry CR, Curnoe D, Chamoli U. 2010. The craniomandibular  
1127 mechanics of being human. *Proc R Soc Lond B Biol Sci* 277:3579-3586.
- 1128 Zink KD, Lieberman DE. 2016. Impact of meat and Lower Palaeolithic food processing  
1129 techniques on chewing in humans. *Nature* (Early View). doi:10.1038/nature16990.
- 1130 Zioupos P, Smith CW, Yuehwei HA. 2000. Factors affecting mechanical properties of bone. In:  
1131 An YH, Draughn RA (editors). *Mechanical testing of bone and the bone-implant*  
1132 interface. Boca Raton: CRC Press. p 65–85.

**Table 1** (on next page)

Landmarks used in the geometric morphometric analysis of human craniofacial shape.

Coordinate data on these landmarks were collected by Baab and colleagues (Baab, 2007; Baab et al., 2010). The landmarks chosen for the analysis performed here are a subset of those used by Baab and colleagues, consisting mainly of facial landmarks. Landmark numbers and descriptions correspond to those in Baab (2007).

Landmark	Number <sup>1</sup>	Landmark	Number <sup>1</sup>
Alare (R, L)	13, 40	Lingual canine margin (R, L)	124, 115
Alveolare	11	M1-M2 contact (R, L)	119, 128
Anterior nasal spine	10	M2-M3 contact (R, L)	120, 129
Anterior pterion (R, L)	24, 51	Malar root origin (R, L)	31, 58
Basion	67	Mid post-toral sulcus	6
Bregma	5	Midline anterior palatine	70
Canine-P3 contact (R, L)	116, 125	Mid-torus inferior (R, L)	21, 48
Center of mandibular fossa (R, L)	97, 103	Mid-torus superior (R, L)	22, 49
Dacryon (R, L)	16, 43	Nasion	8
Distal M3 (R, L)	121, 130	Opisthion	66
Frontomalare orbitale (R, L)	20, 47	Orbitale (R, L)	18, 45
Frontomalare temporale (R, L)	19, 46	P3-P4 contact (R, L)	117, 126
Frontosphenomolare (R, L)	23, 50	P4-M1 contact (R, L)	118, 127
Frontotemporale (R, L)	35, 62	Porion (R, L)	27, 54
Glabella	7	Postglenoid (R, L)	94, 100
Hormion	68	Rhinion	9
Incisivon	71	Root of zygomatic process (R, L)	32, 59
Inferior entoglenoid (R, L)	95, 101	Spheno-palatine suture (R, L)	108, 112
Inferior zygotemporal suture (R, L)	72, 78	Staphylion	69
Infraorbital foramen (R, L)	12, 39	Stephanion (R, L)	34, 61
Inion	1	Superior zygotemporal suture (R, L)	25, 52
Jugale (R, L)	26, 53	Supraorbital notch (R, L)	17, 44
Lambda	3	Temporo-sphenoid suture (R, L)	109, 113
Lateral articular fossa (R, L)	96, 102	Zygomaxillare (R, L)	14, 41
Lateral prosthion (R, L)	114, 123	Zygoorbitale (R, L)	15, 42

1 <sup>1</sup>Landmark numbers correspond to those in Baab (2007).

2

3

4

**Table 2** (on next page)

Geographic distribution of human specimens included in the analysis of craniofacial shape variation.

All specimens are housed at the American Museum of Natural History (AMNH).

<b>Region/Population</b>	<b>N</b>
Aboriginal Australian	9
Khoe-San, South Africa	3
China	6
East Africa	7
Grand Gulch, Utah	10
Greifenberg, Carinthia, Austria	6
Heidenheim, Germany	1
Kakoletri, Peloponnesus, Greece	1
Maori, Waitakeri, New Zealand	4
Mongolia	1
Point Hope, Alaska	12
Southeast Asia	12
Tarnapol, Galicia, Poland	2
Tasmanian	4
Tierra del Fuego, Argentina	3
West Africa	7

1

2

**Table 3** (on next page)

Human crania sorted by their Euclidean distance from the group centroid.

The first 25 specimens represent the most distant from the group centroid, whereas the bottom row represents an “average” representative of human cranial shape based on its close proximity to the centroid. Values in parentheses represent the distances expressed in units of the mean pairwise distance (0.068), which provides information on how much farther a particular cranium is from the centroid than the mean distance. Specimens are coded here following American Museum of Natural History (AMNH) catalog numbers.

<b>Specimen</b>	<b>Region/Population</b>	<b>Distance from centroid</b>
VL/2463 <sup>1</sup>	Khoe-San, South Africa	0.1011 (1.49)
VL/3878 <sup>1</sup>	Greifenberg, Austria	0.0939 (1.38)
99/7889 <sup>1</sup>	Malay Archipelago, SE Asia	0.0918 (1.35)
VL/3818	Greifenberg, Austria	0.0885 (1.31)
VL/269	Tasmanian	0.0881 (1.30)
VL/229	Kalmuk, Western Mongolia	0.0876 (1.29)
VL/408	Mhehe, East Africa	0.0871 (1.28)
99.1/511 <sup>1</sup>	Point Hope, Alaska	0.0871 (1.28)
99/8155	Aboriginal Australian	0.0842 (1.24)
99/6562	Māori, New Zealand	0.0830 (1.22)
VL/271	Tasmanian	0.0824 (1.22)
VL/2470 <sup>1</sup>	Khoe-San, South Africa	0.0788 (1.16)
VL/1902	Māori, New Zealand	0.0777 (1.15)
99.1/490	Point Hope, Alaska	0.0770 (1.14)
99/8165	Aboriginal Australian	0.0767 (1.13)
VL/272	Tasmanian	0.0750 (1.11)
VL3619	Greifenberg, Austria	0.0745 (1.10)
99/7333	Grand Gulch, Utah	0.0741 (1.09)
99/8177	Aboriginal Australian	0.0740 (1.09)
VL/2267	Kakoletri, Greece	0.0733 (1.08)
VL/1729	Tientsin, China	0.0728 (1.07)
VL/1602 <sup>1</sup>	Ashanti, West Africa	0.0727 (1.07)
VL/274	Tasmanian	0.0721 (1.06)
VL/2389	Ashanti, West Africa	0.0721 (1.06)
99/8171	Aboriginal Australian	0.0720 (1.06)
99/7365 <sup>1</sup>	Grand Gulch, Utah	0.0496 (0.73)

1 <sup>1</sup> Specimens selected to be modeled using FEA.

2  
3  
4  
5



**Table 4**(on next page)

Pairwise distances between the 6 human cranial specimens selected for use in finite element analysis.

Values in parentheses represent the distances expressed in units of the mean pairwise distance (0.068). Specimens are coded here following American Museum of Natural History (AMNH) catalog numbers.

	<b>VL/2463</b>	<b>VL/3878</b>	<b>99/7889</b>	<b>99.1/511</b>	<b>VL/2470</b>	<b>VL/1602</b>
<b>VL/2463</b>		0.1634 (1.70) <sup>1</sup>	0.0938 (0.97)	0.1534 (1.59) <sup>1</sup>	0.1083 (1.12)	0.1145 (1.19)
<b>VL/3878</b>			0.1469 (1.52)	0.1304 (1.35)	0.1230 (1.28)	0.1385 (1.44)
<b>99/7889</b>				0.1526 (1.58) <sup>1</sup>	0.1178 (1.22)	0.1029 (1.09)
<b>99.1/511</b>					0.1330 (1.38)	0.1256 (1.30)
<b>VL/2470</b>						0.1049 (1.09)
<b>VL/1602</b>						

1 <sup>1</sup>These represent the greatest pairwise distances in the final sample.

2

3

**Table 5** (on next page)

Muscle force scaling for the ALL-HUM and CHIMPED models of modern human crania.

Muscle forces in Newtons (N) were scaled by model size, where size is represented by model volume in mm<sup>3</sup>. Models are shown here ordered from smallest to largest in size. AT = anterior temporalis, SM = superficial masseter, DM = deep masseter, MP = medial pterygoid.

Variant	Model	Volume (mm <sup>3</sup> )	Volume <sup>2/3</sup>	Muscle Force (N)			
				AT	SM	DM	MP
<b>ALL-HUM</b>	KSAN2	331466	4789.53	128.41	105.15	53.29	108.64
	MALP	364129	5099.22	136.72	111.95	56.73	115.67
	KSAN2	433331	5726.38	153.53	125.72	63.71	129.89
	WAFR	475555	6092.57	163.35	133.75	67.79	138.20
	BERG	489588	6211.84	166.55	136.37	69.11	140.90
	GRGL	557223	6771.52	181.55	148.66	75.34	153.60
	TIGA	655320	7544.59	202.28	165.63	83.94	171.14
<b>CHIMPED</b>	KSAN2	331466	4789.53	556.13	572.02	85.07	189.02
	MALP	364129	5099.22	592.09	609.00	90.57	201.24
	KSAN2	433331	5726.38	664.91	683.90	101.71	225.99
	WAFR	475555	6092.57	707.43	727.64	108.22	240.44
	BERG	489588	6211.84	721.28	741.88	110.34	245.15
	GRGL	557223	6771.52	786.26	808.73	120.28	267.24
	TIGA	655320	7544.59	876.02	901.05	134.01	297.74

1

**Table 6** (on next page)

Results of *in vitro* validation analysis.

Average values and standard deviations for maximum (MaxPrin) and minimum (MinPrin) principal strain magnitudes recorded during three *in vitro* loading trials on the left P<sup>3</sup> biting , the results of a specimen-specific *in silico* (FEA) loading analysis, and an estimate of the error in the FEA, where “error” is represented by the difference between *in vitro* (observed) and *in silico* (expected) results, divided by the expected results. See Fig. S3 – Fig. S7 for site locations. Units are in microstrain ( $\mu\epsilon$ ).

Site	Exp.	MaxPrin	MinPrin	Site	Exp.	MaxPrin	MinPrin
1.	<i>In vitro</i>	15.00 (4.36)	-10.33 (2.08)	8.	<i>In vitro</i>	42.33 (2.08)	-109.67 (3.06)
	<i>In silico</i>	14	-15		<i>In silico</i>	37	-105
	Error	6.67%	45.16%		Error	12.60%	4.26%
2.	<i>In vitro</i>	13.00 (1.00)	-11.67 (0.58)	9.	<i>In vitro</i>	7.67 (0.58)	-2.67 (2.08)
	<i>In silico</i>	10	-10		<i>In silico</i>	8	-4
	Error	23.08%	14.29%		Error	4.35%	50.00%
3.	<i>In vitro</i>	3.33 (0.58)	-5.00 (1.00)	10.	<i>In vitro</i>	45.33 (2.08)	-22.33 (1.15)
	<i>In silico</i>	6	-7		<i>In silico</i>	23	-20
	Error	80.00%	40.00%		Error	49.26%	10.45%
4.	<i>In vitro</i>	30.67 (1.15)	-36.00 (0.00)	11.	<i>In vitro</i>	23.67 (0.58)	-10.67 (3.06)
	<i>In silico</i>	29	-34		<i>In silico</i>	22	-13
	Error	5.43%	5.56%		Error	7.04%	21.88%
5.	<i>In vitro</i>	15.00 (2.00)	-14.67 (1.53)	12.	<i>In vitro</i>	108.00 (2.65)	-281.67 (8.33)
	<i>In silico</i>	19	-12		<i>In silico</i>	115	-238
	Error	26.67%	18.18%		Error	6.48%	15.50%
6.	<i>In vitro</i>	11.67 (0.58)	-7.33 (0.58)	13.	<i>In vitro</i>	38.67 (1.15)	-22.00 (1.00)
	<i>In silico</i>	11	-10		<i>In silico</i>	39	-17
	Error	5.71%	36.36%		Error	0.86%	22.73%
7.	<i>In vitro</i>	42.33 (1.53)	-23.33 (2.25)	14.	<i>In vitro</i>	27.67 (2.08)	-42.33 (3.01)
	<i>In silico</i>	42	-17		<i>In silico</i>	38	-25
	Error	0.79%	27.14%		Error	37.35%	40.94%

1

2

**Table 7** (on next page)

Variation in strain and strain energy density in the ALL-HUM models.

Coefficients of variation for maximum principal strain (MaxPrin), minimum principal strain (MinPrin), shear strain (Shear), von Mises strain, and strain energy density (SED) at the 14 locations examined during premolar (P<sup>3</sup>) and molar (M<sup>2</sup>) biting in the ALL-HUM models of modern human crania. Site numbers follow Figure 4.

Site	Bite	MaxPrin	MinPrin	Shear	von Mises	SED
<b>1</b>	P <sup>3</sup>	56.01	34.39	28.49	27.88	59.08
	M <sup>2</sup>	43.20	28.62	20.78	22.82	50.07
<b>2</b>	P <sup>3</sup>	28.35	41.61	30.51	29.27	78.82
	M <sup>2</sup>	27.61	44.20	29.50	29.04	60.38
<b>3</b>	P <sup>3</sup>	23.83	26.53	22.94	22.97	52.39
	M <sup>2</sup>	25.16	24.29	24.66	24.16	49.48
<b>4</b>	P <sup>3</sup>	15.30	21.39	14.75	14.28	27.78
	M <sup>2</sup>	34.43	22.83	22.73	21.46	36.89
<b>5</b>	P <sup>3</sup>	14.32	13.06	12.77	13.24	26.98
	M <sup>2</sup>	12.50	14.22	11.70	12.06	24.53
<b>6</b>	P <sup>3</sup>	21.74	12.21	11.77	11.89	23.52
	M <sup>2</sup>	17.43	13.56	11.13	12.05	25.11
<b>7</b>	P <sup>3</sup>	12.53	8.26	8.09	7.93	15.97
	M <sup>2</sup>	11.27	6.05	5.78	5.32	11.98
<b>8</b>	P <sup>3</sup>	19.73	2.58	13.87	12.50	25.96
	M <sup>2</sup>	20.48	12.04	12.62	11.88	23.36
<b>9</b>	P <sup>3</sup>	20.78	21.84	18.18	19.30	39.77
	M <sup>2</sup>	12.59	9.28	8.23	8.66	19.36
<b>10</b>	P <sup>3</sup>	11.70	33.05	12.32	11.72	21.21
	M <sup>2</sup>	35.51	22.16	25.60	25.86	50.44
<b>11</b>	P <sup>3</sup>	24.44	37.84	24.15	21.83	36.54
	M <sup>2</sup>	25.53	43.20	28.88	26.73	52.39
<b>12</b>	P <sup>3</sup>	51.04	35.54	39.39	37.44	64.43
	M <sup>2</sup>	52.66	34.33	41.78	40.46	76.44
<b>13</b>	P <sup>3</sup>	28.41	34.42	26.48	25.60	51.87
	M <sup>2</sup>	14.11	20.80	14.37	13.50	28.05
<b>14</b>	P <sup>3</sup>	35.54	22.56	31.16	31.33	68.31
	M <sup>2</sup>	39.93	26.73	35.19	35.33	80.97

1

2

3



**Table 8**(on next page)

Variation in von Mises strain magnitudes: Human vs. Chimpanzee.

Comparisons of the coefficients of variation (CVs) for von Mises strain recorded in the CHIMPED human models and the chimpanzee results from Smith et al. (2015b) at each of the 14 craniofacial sites examined. Results of Fligner-Killeen tests for equal CVs between the species are also presented ( $\alpha=0.05$ ). Comparisons that yielded significant results are shown in bold typeface.

Site		P <sup>3</sup>	M <sup>2</sup>	Site		P <sup>3</sup>	M <sup>2</sup>
<b>1</b>	CV - Human	29.04	22.68	<b>8</b>	CV - Humans	10.14	12.27
	CV - Chimp	25.91	23.63		CV - Chimps	16.54	25.58
	p (same CV)	0.065	0.141		p (same CV)	0.143	0.130
<b>2</b>	CV - Humans	24.34	23.05	<b>9</b>	CV - Humans	14.12	8.03
	CV - Chimps	46.61	47.07		CV - Chimps	25.7	23.58
	p (same CV)	0.122	0.050		p (same CV)	0.069	0.052
<b>3</b>	CV - Humans	19.71	17.75	<b>10</b>	CV - Humans	8.8	15.46
	CV - Chimps	19.81	20.10		CV - Chimps	17.36	15.30
	p (same CV)	0.386	0.369		p (same CV)	<b>0.039</b>	0.290
<b>4</b>	CV - Humans	13.51	21.12	<b>11</b>	CV - Humans	10.6	14.34
	CV - Chimps	29.98	33.20		CV - Chimps	27.76	28.11
	p (same CV)	0.176	0.359		p (same CV)	0.056	0.100
<b>5</b>	CV - Humans	12.89	11.50	<b>12</b>	CV - Humans	38.05	38.76
	CV - Chimps	27.56	29.40		CV - Chimps	28.23	43.35
	p (same CV)	0.156	0.060		p (same CV)	0.147	0.396
<b>6</b>	CV - Humans	18.15	16.51	<b>13</b>	CV - Humans	24.54	10.39
	CV - Chimps	64.99	66.99		CV - Chimps	17.95	17.52
	p (same CV)	<b>0.022</b>	<b>0.022</b>		p (same CV)	0.157	0.207
<b>7</b>	CV - Humans	11.96	12.07	<b>14</b>	CV - Humans	22.78	23.11
	CV - Chimps	55.83	56.63		CV - Chimps	51.99	55.84
	p (same CV)	<b>0.022</b>	<b>0.022</b>		p (same CV)	0.222	0.166

1

2

**Table 9** (on next page)

Bite force production, biting efficiency, and joint reaction forces in the ALL-HUM model variants of human crania.

Bite force (BF), mechanical advantage (MA), working-side TMJ reaction force (RF-WS), and balancing-side TMJ reaction force (RF-BS) for premolar and molar biting. Five of seven ALL-HUM models generated distractive (tensile) reaction forces during molar loading. Therefore, balancing side muscle forces were iteratively reduced by 5% and re-run until distractive forces were eliminated. Bite forces and TMJ reaction forces are in Newtons (N).

Model	Muscle Force	Premolar Bite				Molar Bite			
		BF	MA	RF-WS	RF-BS	BF	MA	RF-WS	RF-BS
GRGL	1118	441	0.39	167.42	349.25	658	0.59	-11.74	329.79
GRGL <sup>1</sup>	1090					642	0.59	-1.37	311.18
GRGL <sup>2</sup>	1062					625	0.59	8.98	292.58
BERG	1026	439	0.43	147.72	281.55	663	0.65	-6.98	249.09
BERG <sup>1</sup>	1000					647	0.65	1.29	234.72
KSAN1	946	378	0.40	121.76	295.69	538	0.57	-17.49	280.57
KSAN1 <sup>2</sup>	898					511	0.57	0.07	249.74
KSAN2	791	333	0.42	106.83	240.30	496	0.63	-18.86	222.80
KSAN2 <sup>2</sup>	751					471	0.63	-4.26	197.88
KSAN2 <sup>3</sup>	732					459	0.63	3.04	185.41
MALP	842	344	0.41	131.09	277.66	537	0.64	-19.85	274.49
MALP <sup>2</sup>	800					510	0.64	-0.99	242.97
TIGA	1246	507	0.41	187.96	373.24	756	0.61	13.68	336.84
WAFR	1006	341	0.34	149.36	298.77	529	0.53	12.64	273.79

1 <sup>1</sup>Model re-run using muscle forces reduced by 5% on the balancing side.

2 <sup>2</sup>Model re-run using muscle forces reduced by 10% on the balancing side.

3 <sup>3</sup>Model re-run using muscle forces reduced by 15% on the balancing side.

4

**Table 10**(on next page)

Von Mises strain magnitudes: Human vs. Chimpanzee.

Results of pairwise comparisons (Mann-Whitney *U*-test) of von Mises strain magnitudes at the 14 locations examined between CHIMPED variants of human FEMs and data on chimpanzees from Smith et al. (2015b). Because of small sample sizes, the “exact” variant of *p* is reported (Mundry and Fischer, 1998). Comparisons that yielded significant results following Holm-Bonferroni correction are shown in bold typeface. When significant, humans were found to exhibit the higher average value, with the exception of locations 13 and 14, where humans were found to exhibit significantly lower strain magnitudes.

Site	Bite	U	z	Exact p
1. Dorsal interorbital	Premolar	9	-1.65	0.0967
	Molar	10	-1.50	0.1265
2. Working dorsal orbital	Premolar	0	-2.93	<b>0.0012</b>
	Molar	0	-2.93	<b>0.0012</b>
3. Balancing dorsal orbital	Premolar	4	-2.36	0.0140 <sup>1</sup>
	Molar	7	-1.93	0.0513
4. Working postorbital bar	Premolar	0	-2.93	<b>0.0012</b>
	Molar	1	-2.79	<b>0.0023</b>
5. Balancing postorbital bar	Premolar	0	-2.93	<b>0.0012</b>
	Molar	0	-2.93	<b>0.0012</b>
6. Working zygomatic arch	Premolar	14	-0.93	0.3660
	Molar	14	-0.93	0.3660
7. Balancing zygomatic arch	Premolar	14	-0.93	0.3660
	Molar	14	-0.93	0.3660
8. Working zygomatic root	Premolar	0	-2.93	<b>0.0012</b>
	Molar	0	-2.93	<b>0.0012</b>
9. Balancing zygo root	Premolar	18	-0.36	0.7308
	Molar	11	-1.36	0.1807
10. Working infraorbital	Premolar	2	-2.64	<b>0.0047</b>
	Molar	7.5	-1.86	0.0565
11. Balancing infraorbital	Premolar	6	-2.07	0.0350 <sup>1</sup>
	Molar	12	-1.21	0.2343
12. Working nasal margin	Premolar	0	-2.93	<b>0.0012</b>
	Molar	1	-2.79	<b>0.0023</b>
13. Working zygomatic body	Premolar	0	-2.93	<b>0.0012</b>
	Molar	1	-2.79	<b>0.0023</b>
14. Balancing zygomatic body	Premolar	0.5	-2.86	<b>0.0017</b>
	Molar	1	-2.79	<b>0.0023</b>

1 <sup>1</sup>Result is significant at  $p \leq 0.05$ .

2

**Table 11**(on next page)

Bite force production, biting efficiency, and joint reaction forces in the CHIMPED model variants of human crania.

Bite force (BF), mechanical advantage (MA), working-side temporomandibular joint reaction force (RF-WS), and balancing-side temporomandibular joint reaction force (RF-BS) for premolar and molar biting. All seven CHIMPED models generated highly distractive (tensile) reaction forces during molar loading that would have increased the chances of joint dislocation and/or injury. Therefore, balancing side muscle forces were iteratively reduced by 5% and re-run until distractive forces were eliminated. Bite forces and TMJ reaction forces are in Newtons (N).

Model	Muscle Force	Premolar Bite				Molar Bite			
		BF	MA	RF-WS	RF-BS	BF	MA	RF-WS	RF-BS
GRGL	3965	1724	0.43	499.82	1189.57	2570	0.65	-208.16	1113.51
GRGL <sup>1</sup>	3569					2316	0.65	-31.26	841.64
GRGL <sup>2</sup>	3469					2252	0.65	12.96	773.68
BERG	3637	1720	0.47	405.08	935.03	2599	0.71	-185.65	819.81
BERG <sup>2</sup>	3183					2277	0.71	-6.72	560.17
BERG <sup>3</sup>	3092					2213	0.71	29.07	508.24
KSAN1	3353	1462	0.44	343.26	1030.37	2080	0.62	-187.95	975.38
KSAN1 <sup>2</sup>	2934					1822	0.62	-0.30	687.33
KSAN1 <sup>3</sup>	2850					1771	0.62	37.23	629.72
KSAN2	2804	1272	0.45	311.70	821.79	1895	0.68	-163.75	757.22
KSAN2 <sup>2</sup>	2454					1658	0.68	-11.46	529.80
KSAN2 <sup>3</sup>	2384					1610	0.68	18.99	484.32
MALP	2986	1358	0.45	384.41	966.38	2118	0.71	-203.31	963.66
MALP <sup>2</sup>	2613					1851	0.71	-2.01	667.11
MALP <sup>3</sup>	2538					1797	0.71	38.25	607.81
TIGA	4418	1941	0.44	564.13	1288.46	2896	0.66	-107.59	1143.16
TIGA <sup>4</sup>	4197					2750	0.66	-13.27	997.33
TIGA <sup>5</sup>	4086					2678	0.66	33.89	924.42
WAFR	3567	1383	0.39	489.34	1103.22	2146	0.60	-61.09	1006.50
WAFR <sup>6</sup>	3478					2091	0.60	-24.01	946.69
WAFR <sup>4</sup>	3389					2036	0.60	13.07	886.88

1 <sup>1</sup>Model re-run using muscle forces reduced by 20% on the balancing side.

2 <sup>2</sup>Model re-run using muscle forces reduced by 25% on the balancing side.

3 <sup>3</sup>Model re-run using muscle forces reduced by 30% on the balancing side.

4 <sup>4</sup>Model re-run using muscle forces reduced by 10% on the balancing side.

5 <sup>5</sup>Model re-run using muscle forces reduced by 15% on the balancing side.

6 <sup>6</sup>Model re-run using muscle forces reduced by 5% on the balancing side.

7

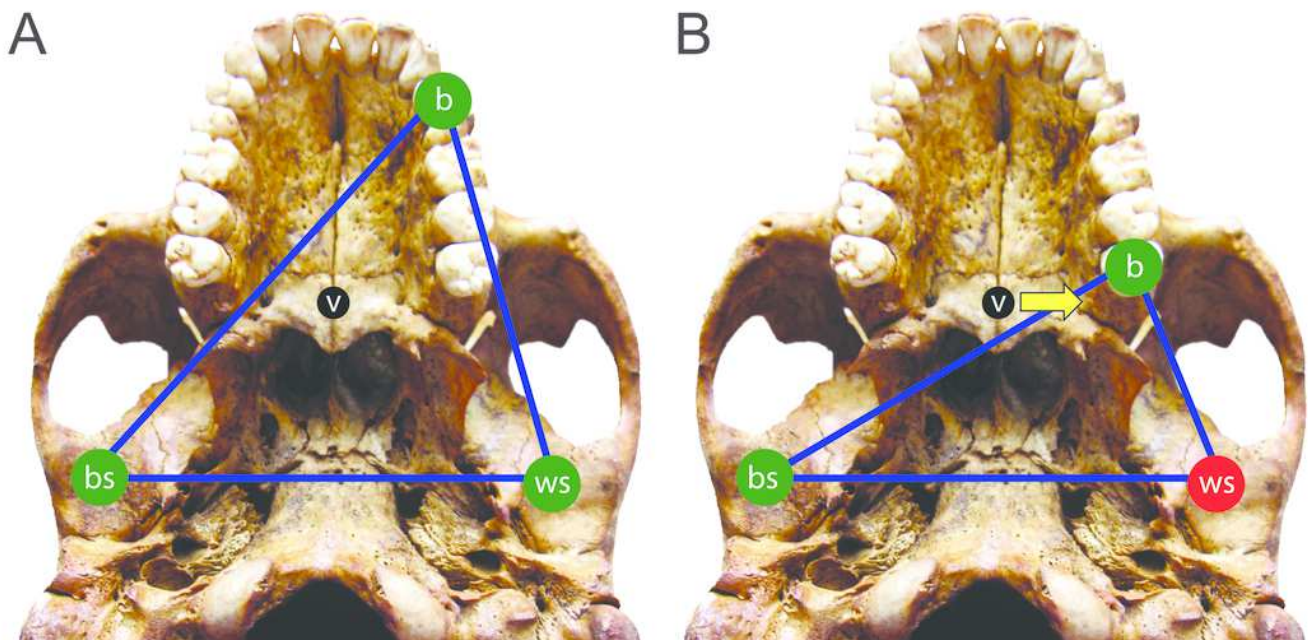
8



## 1

The constrained lever model of jaw biomechanics.

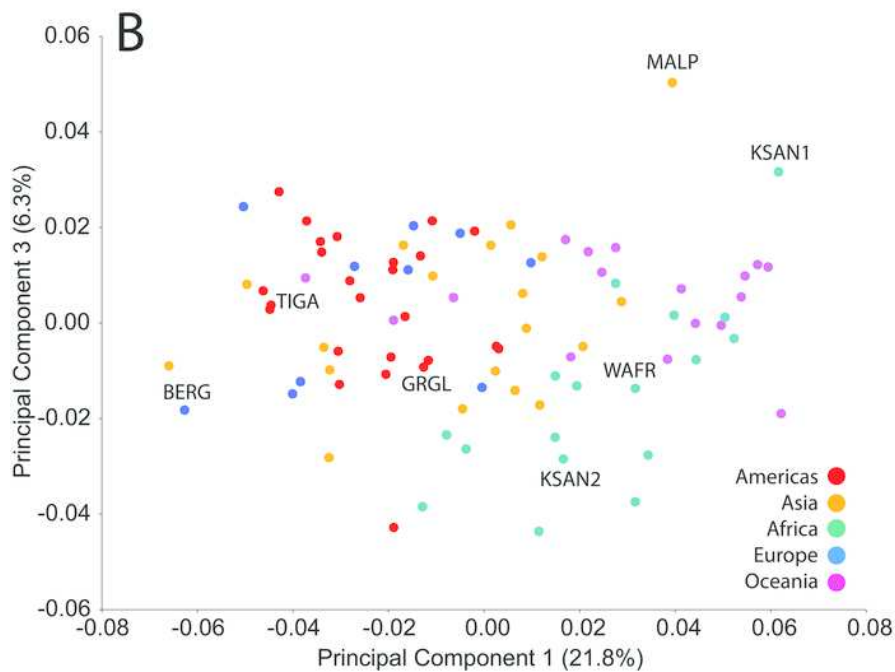
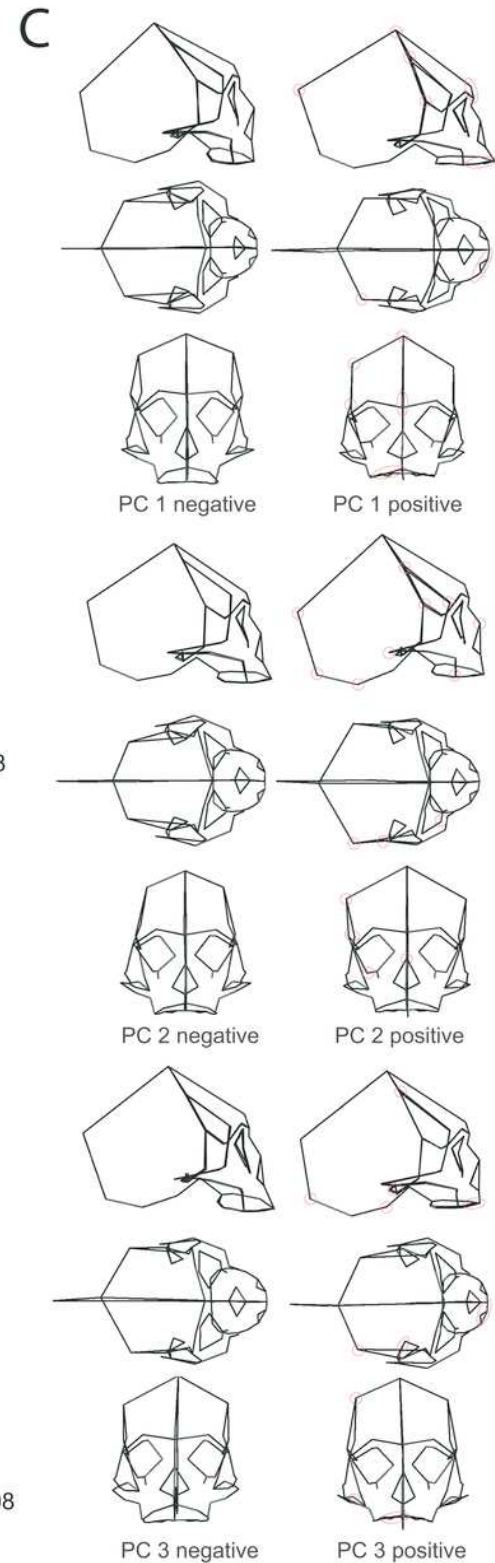
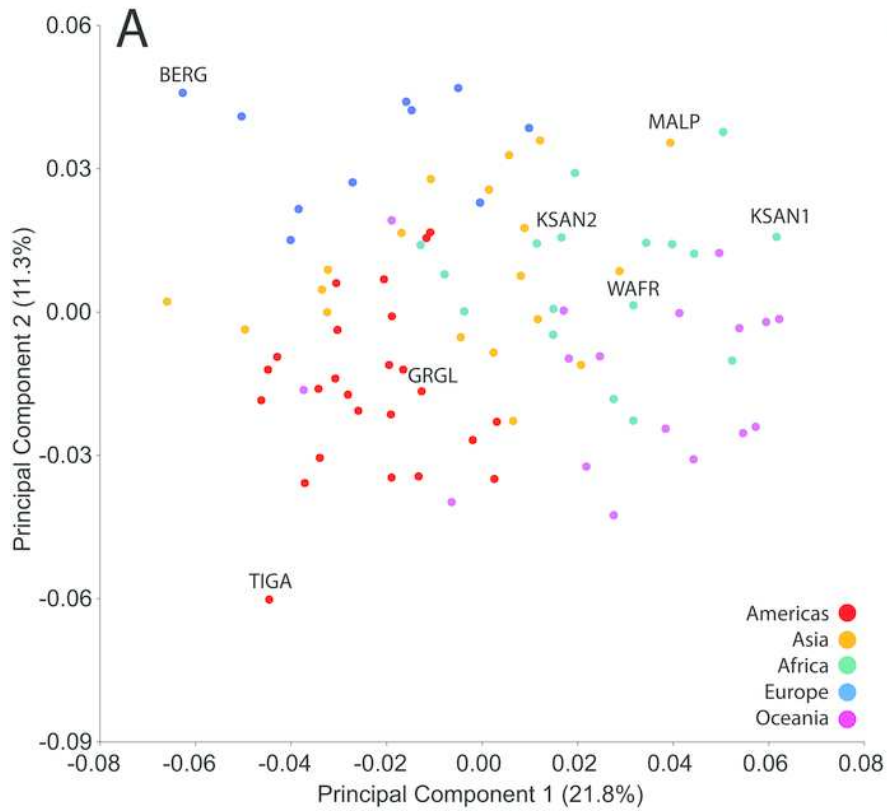
During biting, the bite point (b) and the temporomandibular joints on the working side (ws) and balancing side (bs) form a “triangle of support” that changes shape when biting on different teeth. During a premolar bite (**A**), the resultant vector of the jaw adductor muscles (v) passes through the triangle, producing compression (green circles) at all three points. However, during some molar bites (**B**), the vector falls outside the triangle when the muscles are being recruited equally on both sides of the head, producing compression at the bite point and bs joint, but distraction (red circle) at the ws joint. The recruitment of the balancing side muscles must be lessened in order to eliminate this distraction, thereby causing the vector to shift its position towards the working side and back into the triangle (yellow arrow).



## 2

Principal component analysis (PCA) of human craniofacial shape variation.

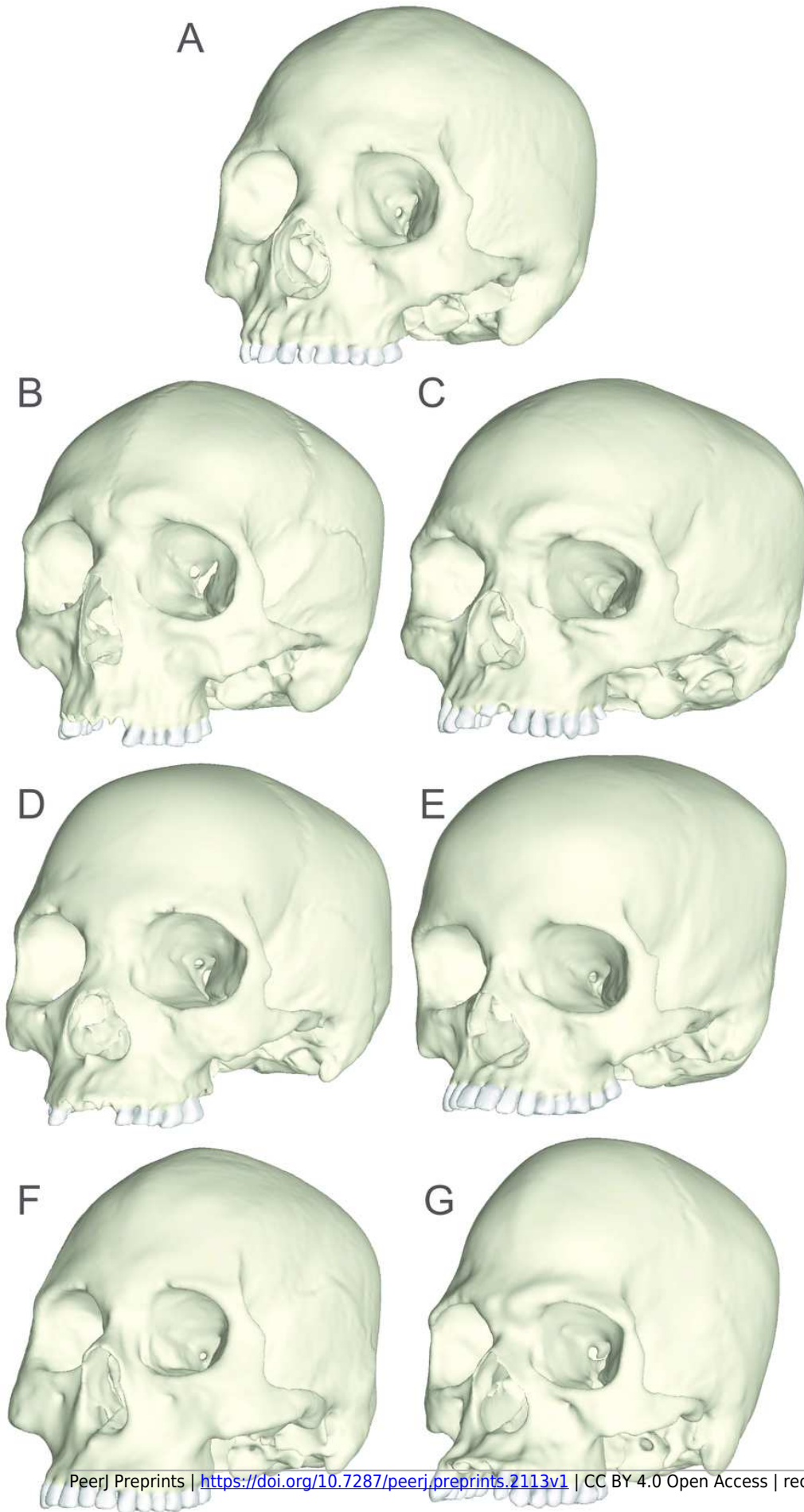
Panels show **(A)** PC1 by PC2, **(B)** PC1 by PC3, and **(C)** wireframes illustrating craniofacial shape change associated with the first three principal components in right lateral, superior, and frontal views. The left and right columns of wireframes represent the negative and positive ends of each component, respectively, scaled to their respective axes. The 10 unique landmarks with the highest loadings for each component are highlighted using a red ellipse on the midline and right side. A single ellipse was used to circle multiple landmarks if they were located close together. Shape differences toward the positive end of PC 1 include: a vertically shorter face with a more projecting brow ridge, a longer and more projecting palate, a more vertical frontal bone that is narrower at pterion, a vault that is expanded posteriorly, and a lower temporal line at stephanion. Shape differences toward the positive end of PC 2 include: a longer cranium with a wider frontal bone, a vault that is angled more postero-inferiorly, wider orbits and a superiorly shifted nasal aperture, and an antero-posteriorly shorter temporal bone. Shape differences toward the positive end of PC 3 include: higher temporal lines at stephanion, a shorter and more orthognathic subnasal region with a less projecting palate, a more inferiorly positioned temporomandibular joint, and a more inferiorly positioned midline cranial base.



# 3

Human models analyzed in the current study.

Models include one “average” cranium, GRGL (**A**), and six “extreme” specimens that differ notably in shape, BERG (**B**), KSAN1 (**C**), KSAN2 (**D**), MALP (**E**), TIGA (**F**), and WAFR (**G**).

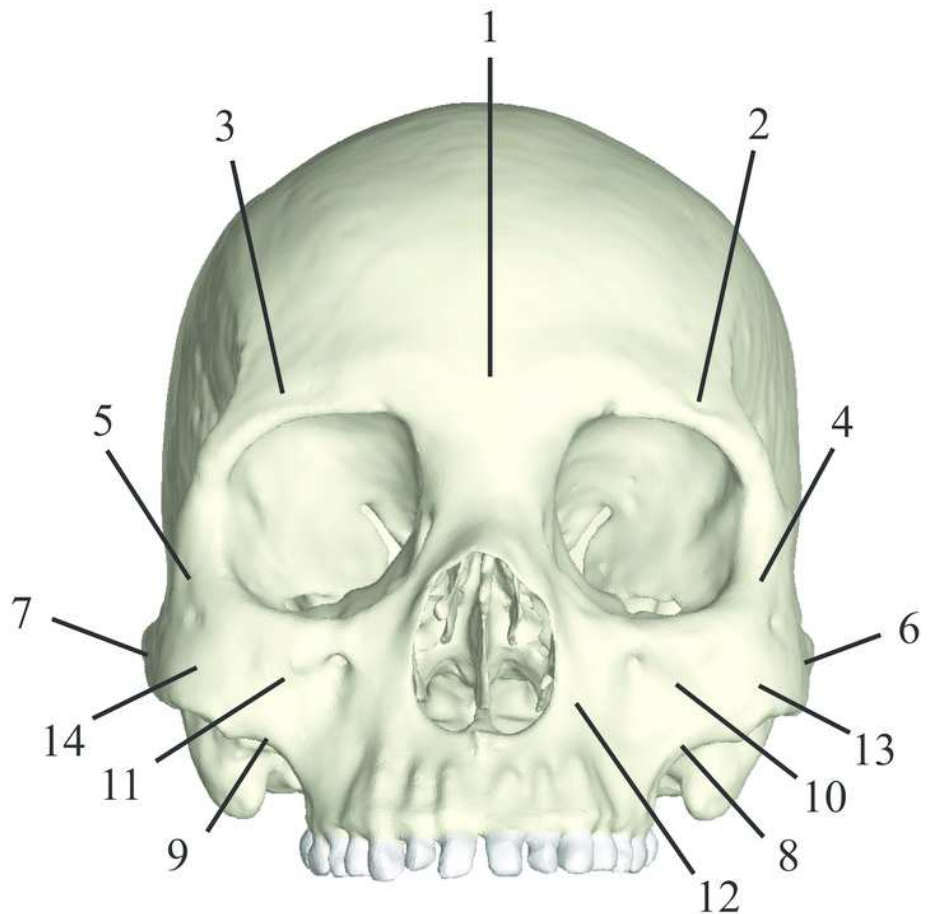


## 4

Key to locations where strains were sampled in finite element models.

Strain data were collected from ALL-HUM and CHIMPED variants of human FEMs from 14 craniofacial sites, following Smith et al. (2015a,b).

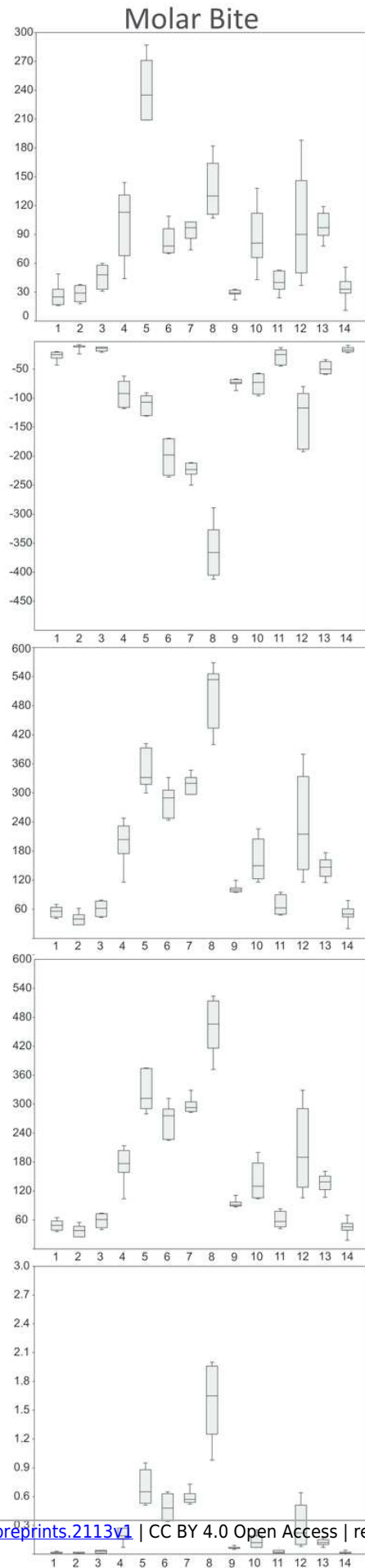
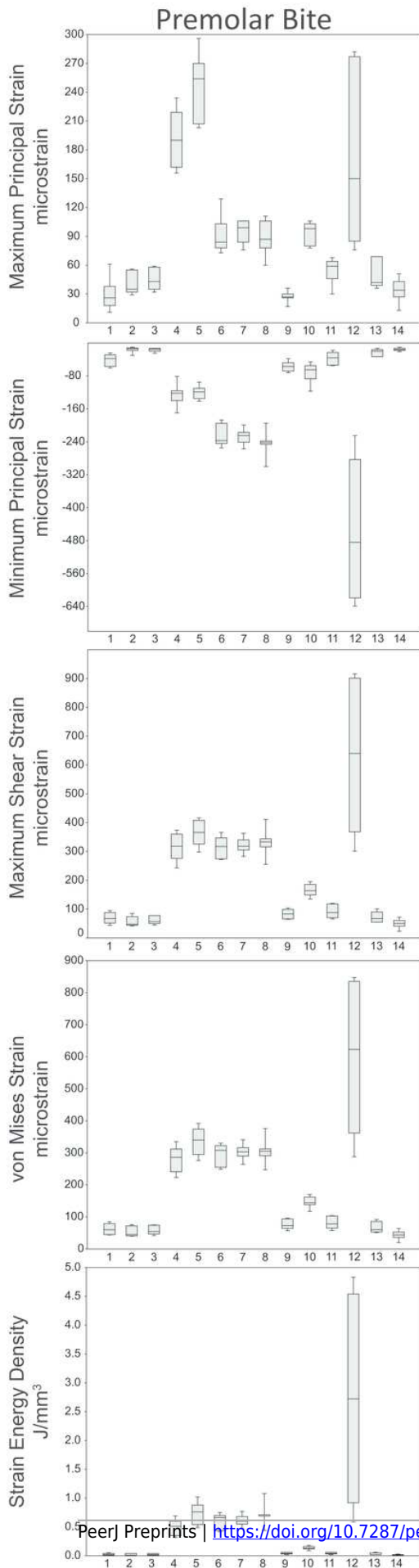
- 1 Dorsal Interorbital
- 2 Working Dorsal Orbital
- 3 Balancing Dorsal Orbital
- 4 Working Postorbital Bar
- 5 Balancing Postorbital Bar
- 6 Working Zygomatic Arch
- 7 Balancing Zygomatic Arch
- 8 Working Zygomatic Root
- 9 Balancing Zygomatic Root
- 10 Working Infraorbital
- 11 Balancing Infraorbital
- 12 Working Nasal Margin
- 13 Working Zygomatic Body
- 14 Balancing Zygomatic Body



# 5

Strain and SED generated by the ALL-HUM models.

Box-and-whisker plots show the minimum, first quartile, median, third quartile, and maximum for strain and SED magnitudes (y-axis) generated by the ALL-HUM models at the 14 sampled locations (x-axis) during premolar (P<sup>3</sup>) and molar (M<sup>2</sup>) biting. Site numbers follow Fig. 4.

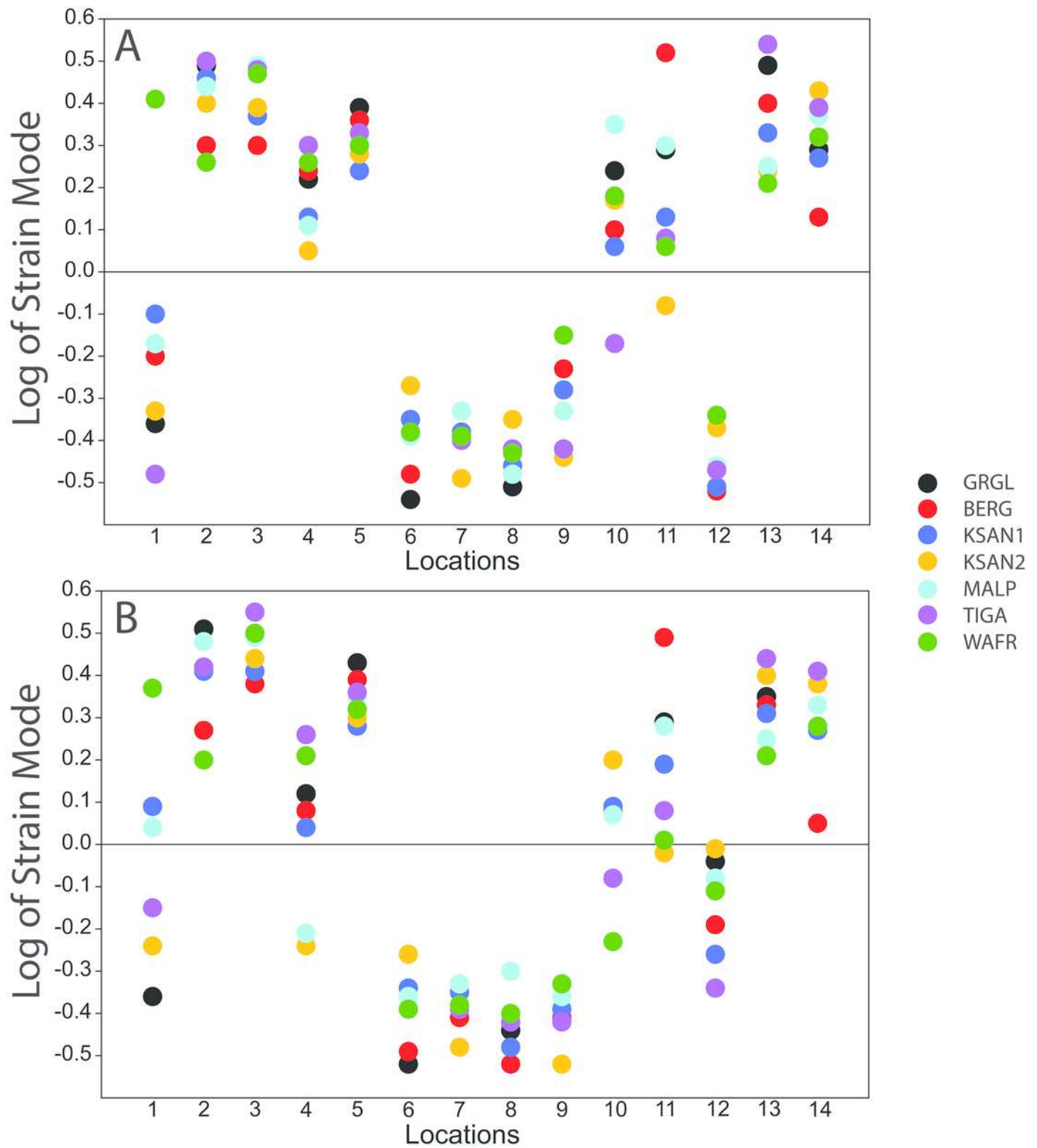




# 6

Strain mode in the ALL-HUM models.

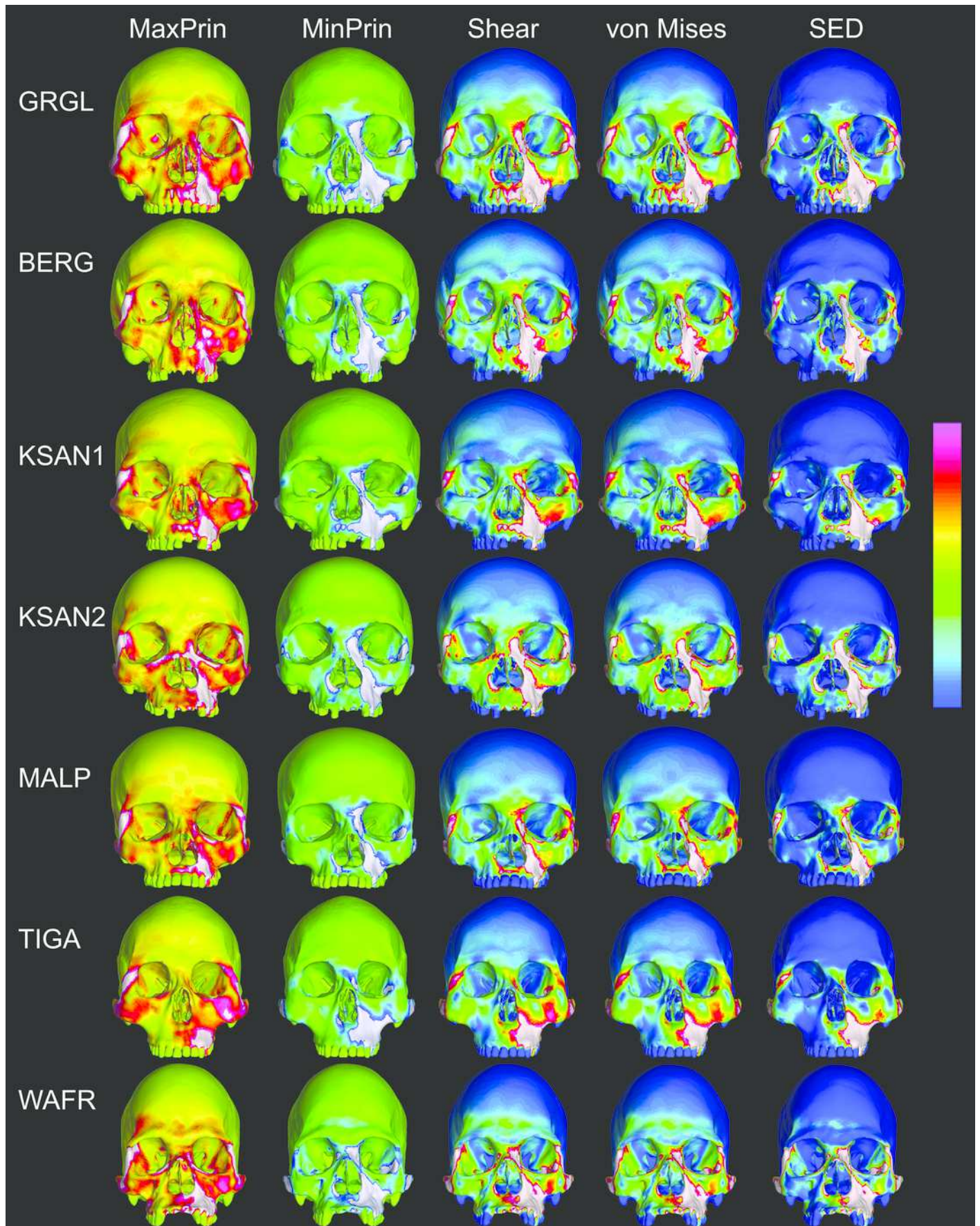
Distribution of strain mode (log of ratio of maximum to minimum principal strain, y-axis) plotted by location (x-axis) in the ALL-HUM models. Plots show **(A)** premolar ( $P^3$ ) and **(B)** molar ( $M^2$ ) biting. Logging the data listed in Tables S2 and S3 centers strain mode data around zero. Values above zero indicate mainly tension, while values below zero indicate mainly compression. Site numbers follow Fig. 4.



## 7

Strain distributions in the ALL-HUM models: P<sup>3</sup> biting.

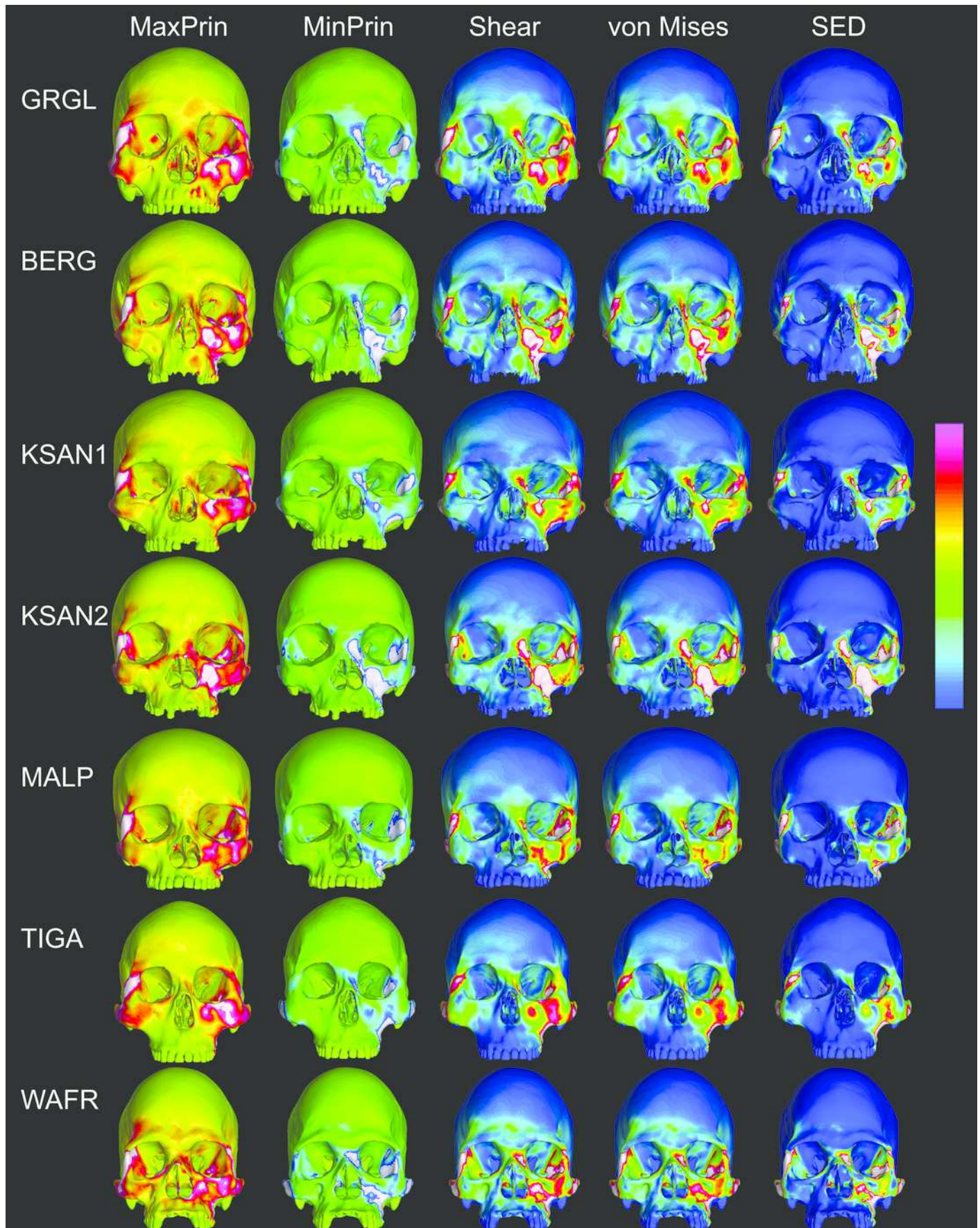
Color maps of strain distributions in the ALL-HUM variants of “extreme” and “average” modern human cranial FEMs during premolar (P<sup>3</sup>) biting. Scales are set to range from -150 – 150  $\mu\epsilon$  for both maximum principal strain (MaxPrin) and minimum principal strain (MinPrin), from 0 – 300  $\mu\epsilon$  for both maximum shear strain (Shear) and von Mises strain (von Mises), and from 0 – 0.5 J/mm<sup>3</sup> for strain energy density (SED). White regions exceed scale. Models are shown at the same height.



## 8

Strain distributions in the ALL-HUM models: M<sup>2</sup> biting.

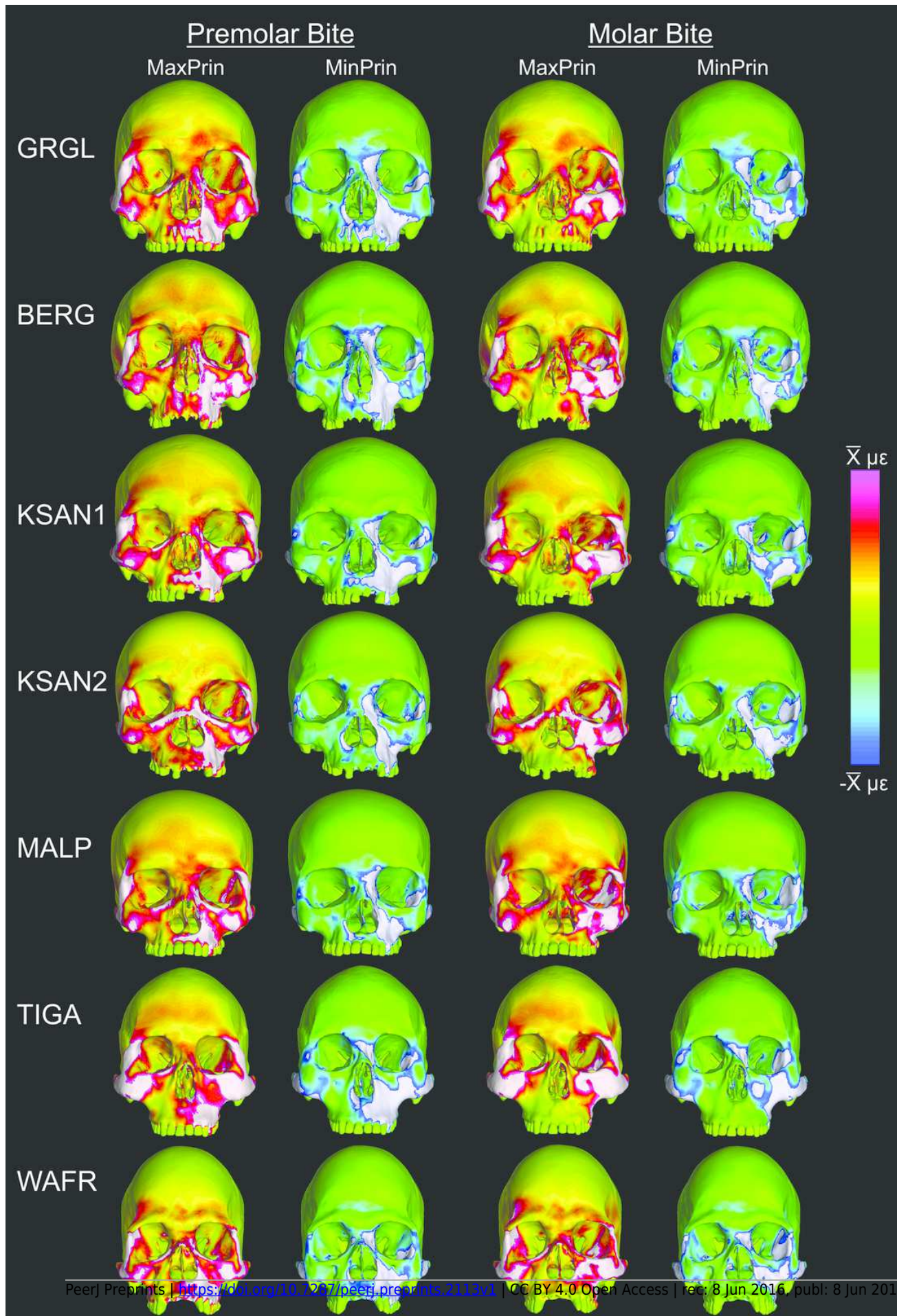
Color maps of strain distributions in the ALL-HUM variants of “extreme” and “average” modern human cranial FEMs during molar (M<sup>2</sup>) biting. Scales are set to range from -150 – 150  $\mu\epsilon$  for both maximum principal strain (MaxPrin) and minimum principal strain (MinPrin), from 0 – 300  $\mu\epsilon$  for both maximum shear strain (Shear) and von Mises strain (von Mises), and from 0 – 0.5 J/mm<sup>3</sup> for strain energy density (SED). White regions exceed scale. Models are shown at the same height.



## 9

Relative strain distributions.

Color maps of “relative” maximum (MaxPrin) and minimum (MinPrin) principal strains in the CHIMPED model variants during premolar ( $P^3$ ) and molar ( $M^2$ ) biting. The scales range from  $-\bar{x}$  to  $\bar{x}$ , where  $\bar{x}$  differs in each image as follows:  $P^3$ , MaxPrin/MinPrin: GRGL, 612/644; BERG, 500/534; KSAN1, 508/603; KSAN2, 593/724; MALP, 520/610; TIGA, 455/498; WAFR, 672/742;  $M^2$ , MaxPrin/MinPrin: GRGL, 505/546; BERG, 468/525; KSAN1, 441/473; KSAN2, 505/546; MALP, 433/458; TIGA, 419/420; WAFR, 530/553. White regions exceed scale.

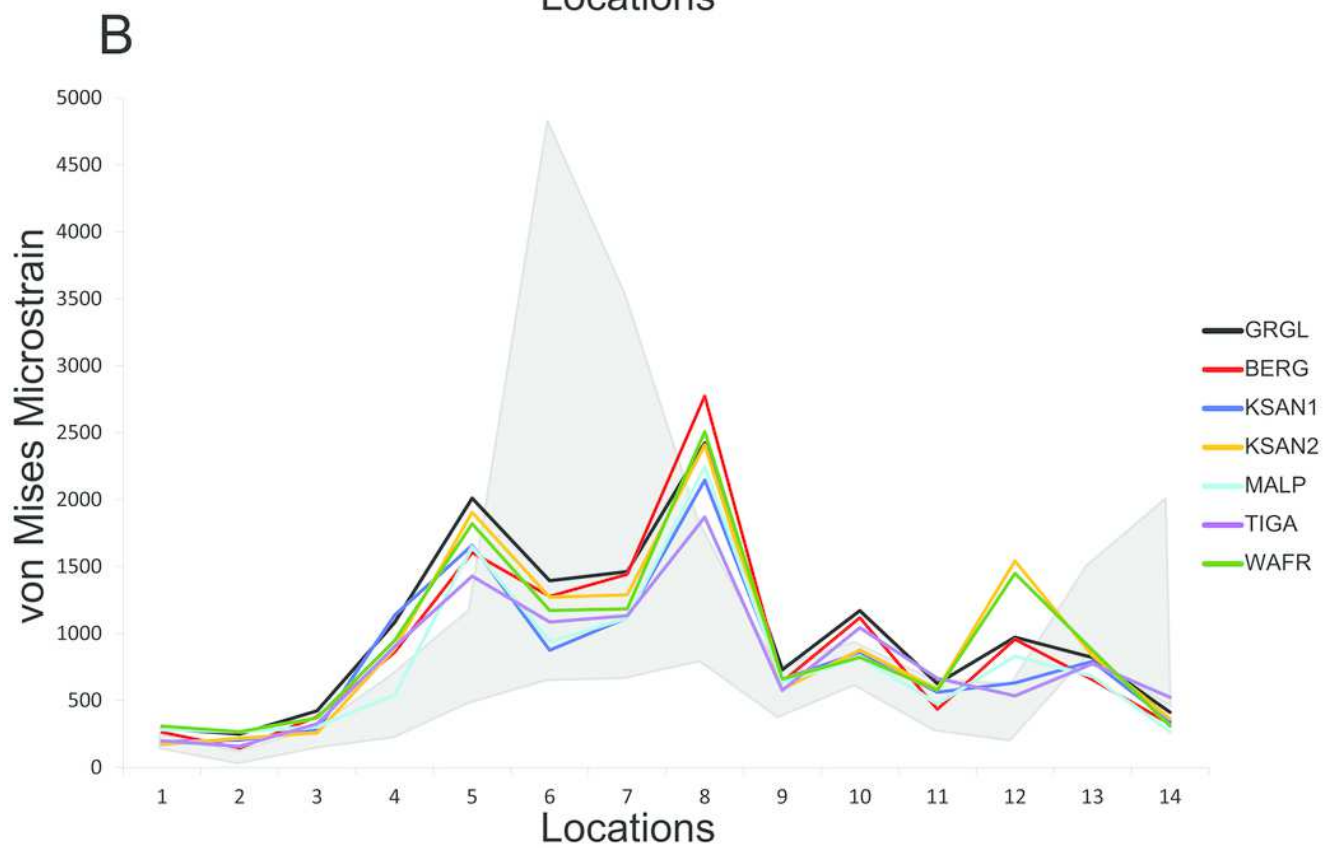
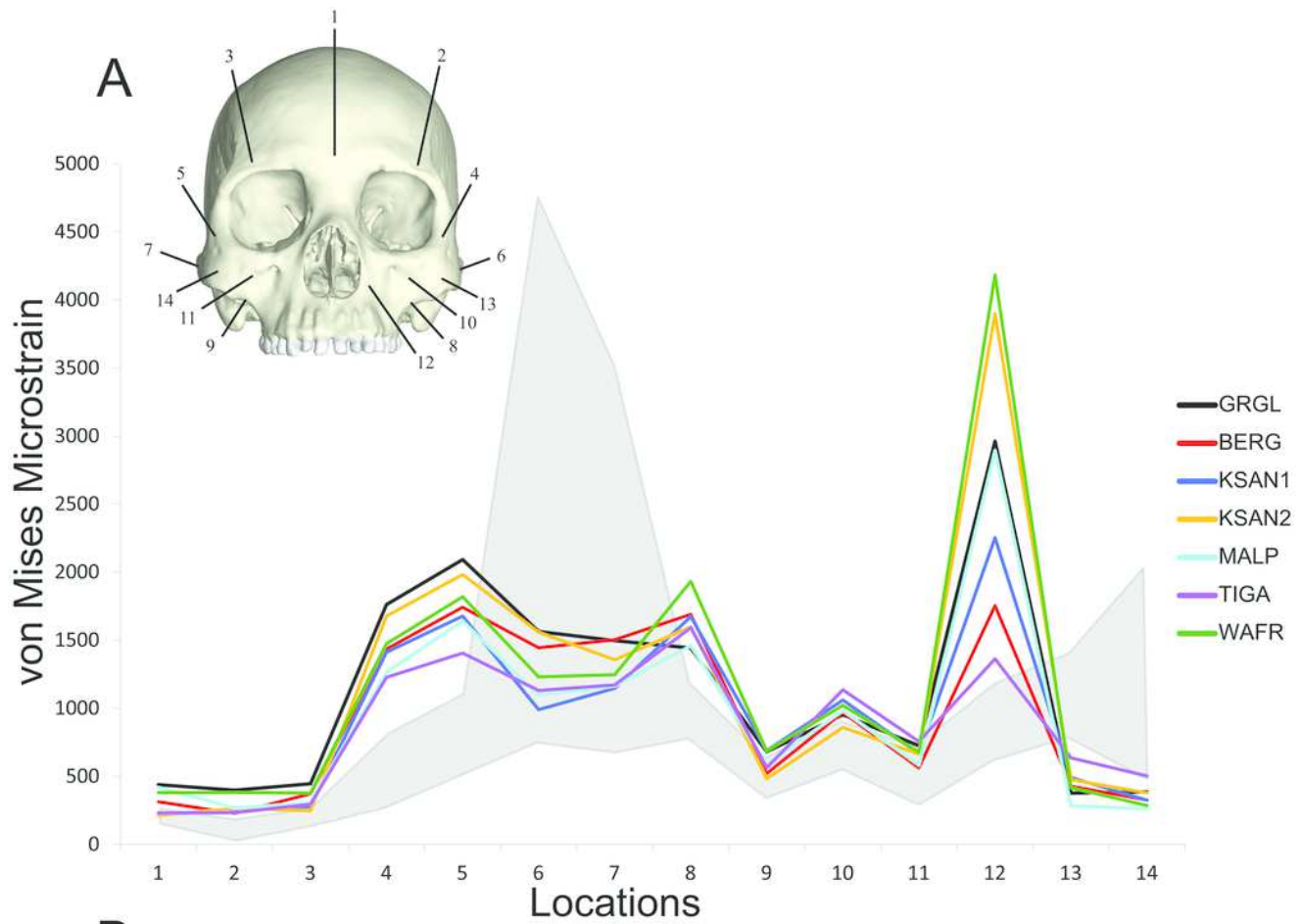




# 10

Line plots of von Mises microstrain generated during simulated biting in finite element models of humans and chimpanzees.

Strain data correspond to **(A)** left premolar ( $P^3$ ) and **(B)** left molar ( $M^2$ ) biting, recorded from 14 homologous locations in the CHIMPED variants of “extreme” and “average” modern human cranial FEMs. The gray region brackets the range of variation observed for chimpanzees by Smith et al. (2015b).



## 11

Biting efficiency: humans vs. chimpanzees.

Box-and-whisker plots show the minimum, first quartile, median, third quartile, and maximum biting efficiency, as quantified using the mechanical advantage (MA), in the CHIMPED variants of human cranial FEMs vs. chimpanzees at **(A)** premolar ( $P^3$ ) and **(B)** molar ( $M^2$ ) bite points. Chimpanzee data is from Smith et al. (2015b).

